e-Prime - Advances in Electrical Engineering, Electronics and Energy 9 (2024) 100693

Contents lists available at ScienceDirect

e-Prime - Advances in Electrical Engineering, Electronics and Energy

journal homepage: www.elsevier.com/locate/prime

Numerical study of a water-based photovoltaic-thermal (PVT) hybrid solar collector with a new heat exchanger

Yassine El Alami [a], Ali Lamkaddem [a], Rachid Bendaoud [b], Sofian Talbi [c], Mohamed louzazni [a], Elhadi Baghaz [a,*]

[a] Laboratory of Electronics, Instrumentation and Energetic, Faculty of Sciences, Chouaïb Doukkali University, B.P 20, El Jadida, Morocco
[b] Interdisciplinary Laboratory for Research in Science, Education, and Training, Higher School of Education and Training-Berrechid, Hassan First University, Berrechid, Morocco
[c] LPTPME Laboratory, Department of Physics, Faculty of Sciences, Mohammed 1st University, Morocco

ARTICLE INFO

Keywords:
PVT collector
Conjugate heat transfer
Performance
Finite element method
COMSOL multiphysics®

ABSTRACT

Based on the latest information provided by researchers, previous studies have identified two major gaps in the literature: the lack of research on channel-box PVT collectors (PVT-Cs) and the absence of studies on the surface temperature distribution for these systems. To fill these gaps, we proposed a new channel-box PVT-C. We then numerically evaluated its performance, examining its energy aspects under various operating conditions. This evaluation was carried out using COMSOL Multiphysics® software, based on the finite element method (FEM). In addition, we validated our 3D numerical model by comparing it with numerical and experimental data in the literature. The results of this study show that increasing the fluid flow rate increases power and electrical efficiency (EE), and that the optimum cooling water flow rate is around 180 L/h. In addition, the overall efficiency (OE) increases with solar irradiation. Furthermore, the electrical power (EP) increases from 37.06 W to 140.48 W for the PV system, and from 38.45 W to 187.02 W for the PVT-C, when the irradiation increases from 2×10^2 to 10^3 W/m^2, while maintaining an optimum flow rate of 180 L/h. In terms of efficiency, the PVT-C has an electrical, thermal and overall efficiency of approximately 12.11 %, 78.59 % and 90.7 % respectively for an irradiation of 10^3 W/m^2. However, the EE of the PV panel is only 9.09 %, or 3 % less than the PVT-C.

1. Introduction

Today, global energy demand is rising steadily as a result of population growth, industrialization and economic improvement [1,2]. A significant proportion of this demand is met by the use of fossil fuels, it causes a considerable amount of greenhouse gas emissions and contributes to global warming. Moreover, fossil fuel reserves are rapidly decreasing as a non-renewable resource, forcing humanity to explore new energy sources to ensure its survival and prosperity [3]. Solar energy emerges as the most hopeful form of renewable energy, and can be harnessed in two forms : solar thermal energy, gathered through solar thermal collectors, and electrical energy generated by PV panels [4]. However, during this process, a certain amount of heat is also generated, which can have an impact on the performance and lifespan of solar cells [5,6]. When the operating temperature of a cell increases, the band gap of the intrinsic semiconductor shrinks. This has several consequences: firstly, it allows the cell to absorb more incident light, encouraging the generation of mobile charge carriers and leading to an increase in the short-circuit current (I_{sc}). On the other hand, this leads to a reduction in the open circuit voltage (V_{oc}), which in turn leads to a reduction in EE. Relevant research has already shown that a 1 °C increase in solar cell temperature (TC) reduces the EE of the PVT-C by 0.3 to 0.5 % [7,8]. To solve this problem, PVT hybrid solar collectors have been proposed. These collectors make it possible to use both the heat and electrical energy produced by the PV solar cells, thus increasing the OE of the system [9]. The main objective of the PVT-C is to optimize the EE of the PV panel by maintaining lower temperatures.

Over the last decade, a great deal of numerical and experimental research has been conducted to study the design and evaluate the performance of PV and PVT hybrid systems. Fudholi et al. [10] examined the performance of various types of solar absorber, including sheet flow, direct flow and spiral flow models. The results show that, at an irradiance of 8×10^2 W/m^2 and a volume FR of 147.6 L/h, the spiral-flow absorber has overall efficiencies of 68.4 %, 13.8 %, and 54.6 % for total, electrical, and thermal efficiency, respectively. Poredoš et al. [11]

* Corresponding author.
E-mail address: baghaz.e@ucd.ac.ma (E. Baghaz).

https://doi.org/10.1016/j.prime.2024.100693
Received 6 May 2024; Received in revised form 4 June 2024; Accepted 15 July 2024
Available online 16 July 2024

Nomenclature

PV	Photovoltaic
PVT	Photovoltaic thermal
PVT-C	photovoltaic thermal collectors
FEM	Finite element method
AZ	Arrival zone
EZ	Exchange zone
VZ	Evacuation zone
FR	Flow rate
EE	Electrical efficiency
TE	Thermal efficiency
OE	Overall efficiency
CT	Cell temperature
A	Area of PV surface (m^2)
c_p	Specific heat at constant pressure (J Kg^{-1} K^{-1})
G	Solar irradiance (W m^{-2})
k	Thermal conductivity (W m^{-1} K^{-1})
$\dot{m}$	Volume flow rate (L h^{-1})
p_{sc}	Packing factor (%)
E_{in}	Received energy by solar cell (W)
E_p	Electrical power (W)
E_{th}	Thermal energy (W)
T_{out}	Temperature of output water (°C)
T_{sc}	Temperature of solar cell (°C)
T_{ted}	Temperature of tedlar (°C)
T_s	Surface temperature, (°C)
T_g	Temperature of glass (°C)
v_{in}	Input velocity of water (m s^{-1})
A_f	cross-sectional area of the pipe inlet (m^2)
R_e	Reynolds number
u, v, w	components of velocity vector (m s^{-1})

Greek Symbols

ρ	Density (Kg m^{-3})
η_{el}	Electrical efficiency
η_{th}	Thermal efficiency
η_g	Overall efficiency
υ	cinematic viscosity of the water (m^2 s^{-1})

carried out an experimental and numerical evaluation to measure the performance of different configurations of PVT units equipped with roller-bonded absorber plates, using water as the working fluid. Three channel configurations were studied: bionic, parallel and series. Using thermal-hydraulic simulations, they found that the bionic absorber achieved the lowest temperature for the water leaving the absorber. In addition, it offered significant advantages in terms of pressure losses, which were significantly lower than those of the parallel configuration. What's more, the unit fitted with a bionic channel offered optimum energy efficiency. Kazem et al. [12] investigated the EE and TE of three distinct PVT flow configurations (direct flow, sheet flow and spiral flow) with conventional PV systems. The results of the study show that the spiral system has the best EE, followed by the direct flow system and the sheet system. These same trends are also found for the TE and OE of the systems studied. Sheshpoli et al. [13] have carried out both numerical and experimental studies to evaluate different PVT hybrid panel configurations. The objective was to determine the ideal cooling tube arrangement for a given panel. The results of the study confirmed that the use of the serpentine tube configuration resulted in a significant improvement in TE (48.4 %) and EE (7.3 %) compared to the uncooled configuration. Aste et al. [14] carried out a comparative study between two designs of PVT units: serpentine tube absorbers and parallel tube absorbers. The results of the study revealed a non-uniform temperature distribution in the tubes of the two types of absorbers. Additionally, the serpentine tube absorber exhibited a steeper temperature gradient than that of the parallel tube absorber. Furthermore, the performance of the parallel tube absorber was found to be superior to that of the serpentine tube absorber. Ibrahim et al. [15] designed and fabricated two PVT-C's in their study. The first collector adopts a spiral flow configuration, while the second is a single-pass rectangular tunnel absorber. Results achieved indicate that the spiral flow design offers the best performance, with higher TE and EE. Verma et al. [16] carried out a comparison between a planar spiral solar thermal collector and the traditional harp design. The results showed that at a volume FR of 93.6 L/h, the spiral design showed a significant 21.45 % improvement in TE over the harp design. Nahar et al. [17] developed a novel spiral heat exchanger. They attached this heat exchanger directly to the PV panel using thermal paste, taking into account copper and aluminum tubes. The results of the study indicate that the performance of copper and aluminum materials is almost similar. Using the flow channel proposed by Nahar et al. [17], the module temperature decreases by 42 °C, and the EE of the PV module increases by 2 %. Shahsavar [18] carried out an extensive performance comparison between a modified sinusoidal serpentine collector and a standard serpentine collector. The results showed a significant improvement in TE of 30.63 % and a slight increase in EE of 2.32 % compared to PVT using a standard serpentine collector. These findings highlight the remarkable benefits of the modified sinusoidal serpentine collector in terms of TE, while emphasizing that its impact on EE remains modest. Sopian et al. [19] carried out a comparative study of three PVT water collectors in terms of TE. The collectors studied were equipped with a direct-flow, a parallel-flow and a split-flow collector. The results showed that the split-flow PVT-C outperformed the other two in terms of TE. Nahar et al. [4] developed a PVT-C with a new design for the heat exchanger, eliminating the conventional absorber plate. Numerical simulations and experimental results are in good agreement. For an irradiance of 10^3 W/m^2 and input and ambient temperatures of 34 °C, the maximum OE of the PVT-C obtained by simulation is 84.4 % and that obtained experimentally is 80 %. Herrando et al. [20] studied a water PVT-C with a polycarbonate flat box configuration. Using COMSOL Multiphysics simulation, they evaluated the performance of the PVT's sheet and tube heat exchangers as well as the flat box heat exchanger. The results demonstrate a 15 % reduction in the linear heat loss coefficient. The flat box design offers advantages, including a 9 % decrease in weight and a 21 % reduction in capital costs.

According to the cited literature and studies [8,21–25], most research has focused on sheet and tube PVT-Cs. These systems have a small heat exchange surface area, which results in high thermal resistance, limiting the heat extraction capacity in the tube [26,27]. This in turn results in lower thermal and electrical efficiencies. In addition, the spacing between hollow tubes is a crucial parameter. Greater spacing leads to uneven temperature distribution, which affects the lifetime of solar cells. To remedy these problems, the use of a channel-box PVT-C offers a solution, thanks to a larger heat exchange surface. However, according to the literature, these systems are rarely considered.

Based on the authors' most recent information, previous studies have identified two gaps in the literature: (a) the lack of research into box-channel PVT-Cs; (b) the lack of research into surface temperature distribution and pressure drop for these systems.

In light of these gaps, the aim of this study is to propose a new structure for the channel-box heat exchanger, aimed at significantly improving convective exchange. This approach capitalizes on the fact that almost the entire surface is in direct contact with the fluid, unlike sheet and tube PVT-Cs, which feature a small contact area between the sheet and the tube. In addition, this proposal seeks to solve the problem

of temperature inequality, which impacts the durability of PV panels.

The main contributions of this study can be synthesized as follows:

- To study the impact of different operational conditions, such as flow rate (FR) and solar irradiation levels, on the temperature of the PVT-C and on its EE, TE and OE.
- To evaluate the performance of the proposed system in terms of power and energy.
- Comparison of the results of this study with experimental and numerical data available in the literature to confirm the reliability of the proposed system.

The system examined in this study is innovative and has not been studied before, making the results obtained crucial for the advancement of cooling technologies in the field of PVT-Cs.

This document is structured into four distinct sections. In the first section, a brief summary of the literature on PVT-Cs is given. The second section highlights the methodology and 3D numerical modeling employed in this study. The third section analyzes the results obtained, including their comparison with existing data in the literature. Finally, the conclusions are presented in the fourth section.

2. Methodology

2.1. Description of the new heat exchanger design

The new heat exchanger configuration presented in this study is composed of three main zones: the first is dedicated to the coolant inlet (AZ), the second to heat exchange (ZE), and finally, the third to fluid evacuation (VZ) (Fig. 1(a)). The cooling fluid flows through the heat exchanger in order to utilize the heat produced by the PV module. following a continuous route from the AZ to the VZ, passing through the EZ. When it reaches the AZ, it initially occupies this zone before entering the channels. Similarly, it can also flow freely towards the VZ. This approach ensures uniform fluid distribution in the channels, covering the entire EZ. The EZ consists of a alveolar plate (Fig. 1(b)), comprising a flat top wall in contact with the rear of the PV module, and a bottom wall. These walls have a thickness of 0.4 mm, which facilitates the optimum transfer of the heat between the PV module and the circulating cooling fluid within the channels. In addition, the alveolar plate has openings in its bottom wall, establishing the connection of each channel to the AZ and VZ respectively. The exchanger consists of 94 rectangular channels designed to maintain an efficient thermosiphon effect between the AZ and VZ. It is also equipped with two collectors ensuring the distribution of water in these channels. Each of these collectors is shaped like a rectangle extending across the width of the alveolar plate. They connect to the alveolar plate at one of the openings, and are fitted with a non-welded connector facing outwards from the panel. According to

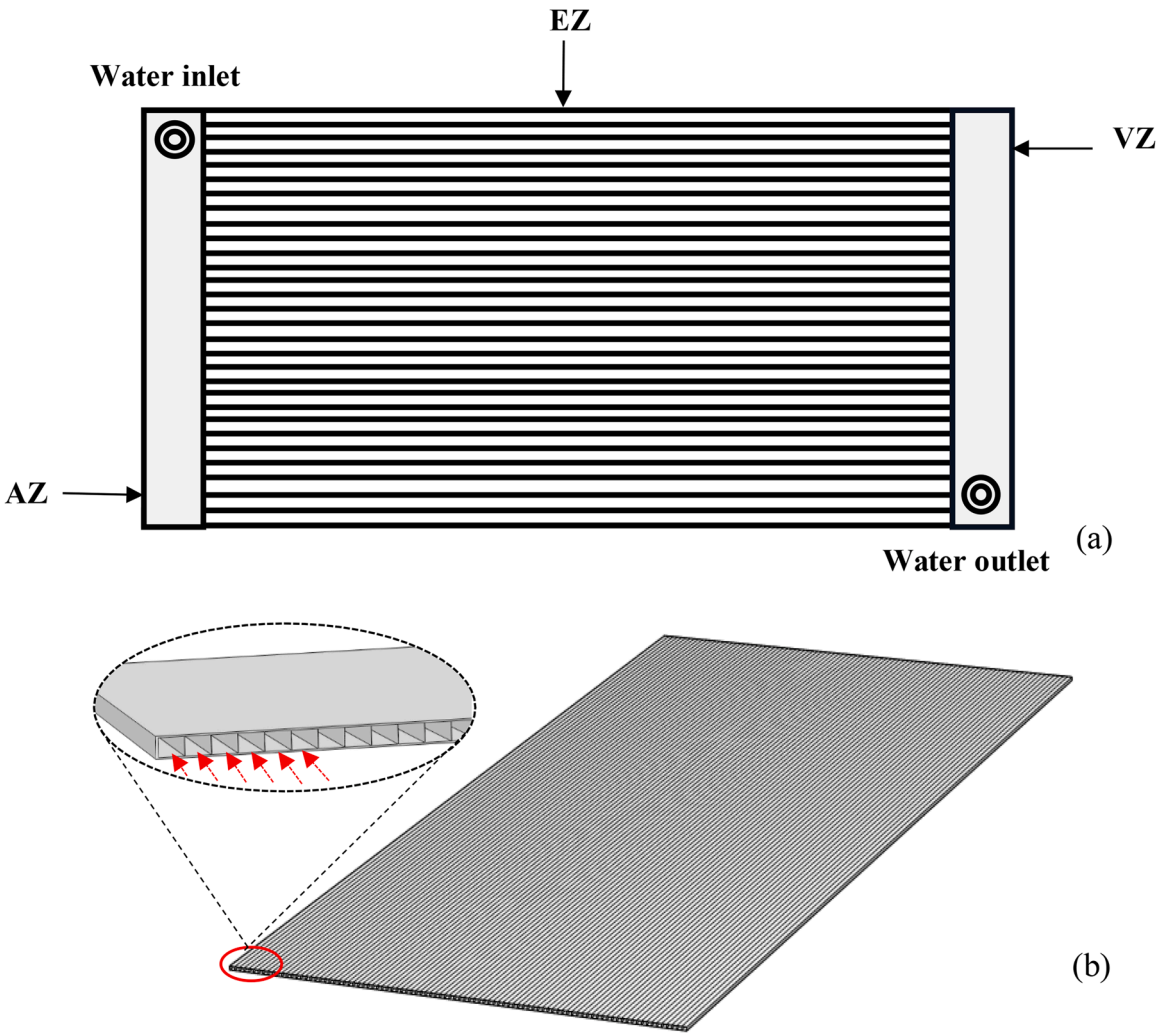

Fig. 1. (a) Heat exchanger configuration, (b) schematic view of the alveolar plate used.

Fig. 1(a), the new heat exchanger's output is located on the right side and its inlet is on the left. The separate parts of the PVT-C are shown in Fig. 2, which includes the PV cell, the Tedlar layer, two transparent layers of ethyl vinyl acetate (EVA), and the glass cover plate. The heat exchanger consists of two distinct zones: a solid zone composed of aluminum and a fluid zone where water flows inside the solid zone. The momentum, and heat conservation equations are solved numerically using the FEM method that was developed using the COMSOL software® [17]. In this numerical study, you will find a description of the materials used, as well as their design parameters and thermo-physical properties, which are listed in Tables 1 and 2.

Table 1
Materials and thermal properties of PVT-C [4,8,28].

Materials	Layers	Thickness (mm)	k [W/(m. K)]	ρ [Kg/m^3]	C_p [J/(kg. K)]
Glass	Top cover	3	1.8	2500	500
EVA	Encapsulant	0.3	0.311	950	2090
Silicon	Solar cell	0.5	148	2329	700
Tedlar	Bottom cover	0.1	0.15	1200	1250
Aluminum	Heat exchanger	0.4	237	2700	900
Fluid	Water	–	0.68	998	4200

Table 2
Parameters of the PVT-C [8,4,29,30].

Parameters	Values
The collector length (mm)	1960
The collector width (mm)	960
Solar irradiance $G(W/m^2)$	2×10^2–10^3
Inlet volumetric FR $\dot{m}(L/h)$	30–210
Inlet temperature T_{in}(°C)	29
Ambient temperature T_{amb}(°C)	25
Reference temperature T_r(°C)	25
PV efficiency η_{sc}(%)at STC	13
solar cell absorptivity α_{sc}	0.9
Packing factor of solar cell P_{sc}	0.95
Glass cover transmissivity τ_g	0.96
Glass emissivity ε_g	0.04
Thermal efficiency coefficient of the solar cell $\mu_{sc}(\%/^{\circ}C)$	−0.0045
Heat transfer coefficient from glass to air $U_{ga}(\mathrm{Wm^{-2}K^{-1}})$	7.14
Heat transfer coefficient inside PVT surfaces $U_t(\mathrm{Wm^{-2}K^{-1}})$	150

2.2. Method of analysis

2.2.1. Numerical and mathematical calculation

When PV and PVT solar panels are placed in a given environment, they absorb a large amount of solar energy. The calculation of the total amount of energy received by these panels takes place as follows [4,31]:

$$E_{in} = \tau_g \alpha_{sc} p_{sc} GA \tag{1}$$

Electrical energy obtained from the energy absorbed by the PV cell, expressed by [4,32,33] :

$$E_p = \eta_{sc} \tau_g \alpha_{sc} p_{sc} GA(1 - \mu_{sc}(T_{sc} - T_r)) \tag{2}$$

The temperature of the PV cell determined by equation provided bellow [29]:

$$T_{sc} = \frac{P_{sc}.G(\tau_g.\alpha_{sc} - \eta_{sc}) + (U_{ga}T_{amb} + U_t T_{ted})}{(U_{ga} + U_t)} \tag{3}$$

The subsequent equation can be employed to determine the thermal

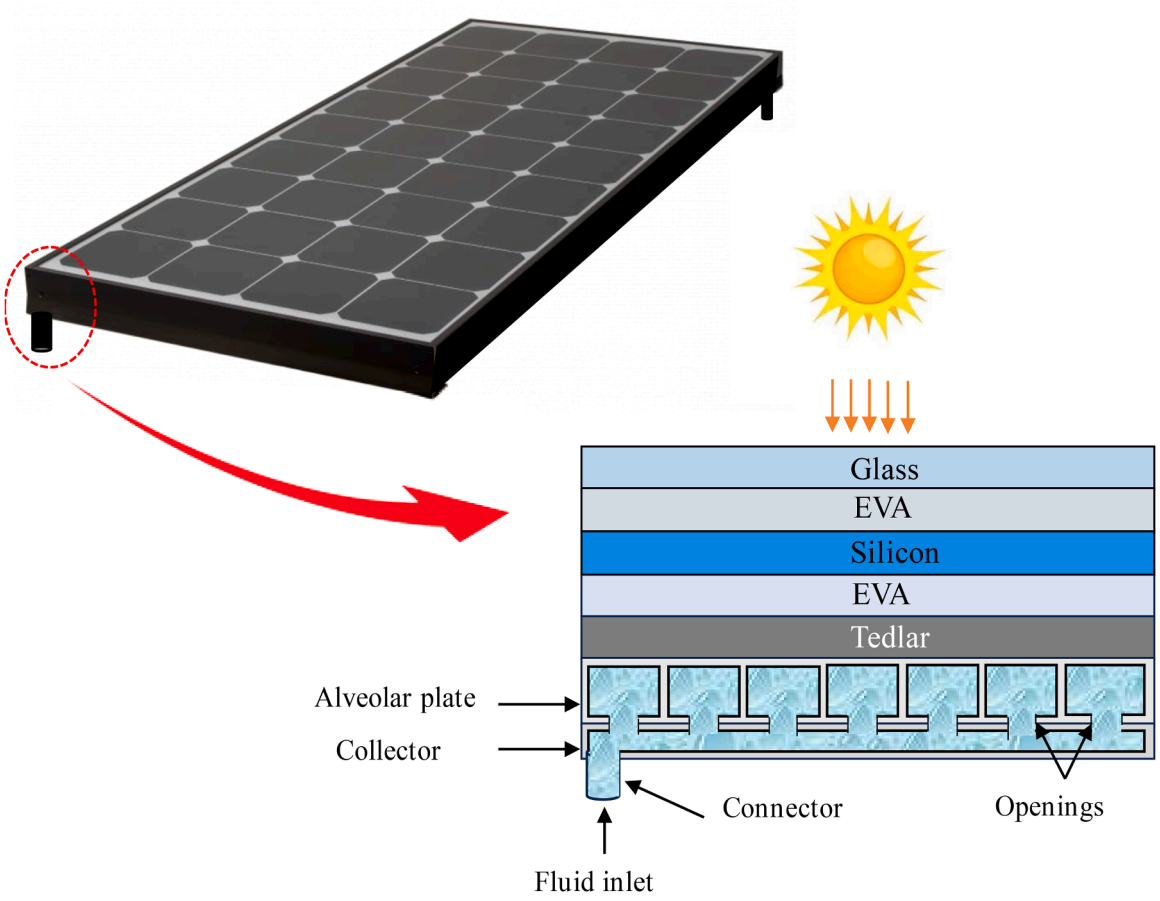

Fig. 2. Detailed diagram of the PVT-C.

energy harvested from the PV panel through the fluid [34]:

$$E_{th} = \dot{m}C_f(T_{out} - T_{in}) \tag{4}$$

the fluid's volume FR given by [4]:

$$Q = A_f v_f \tag{5}$$

Where A_f is the cross-section of the input velocity and is defined by:

$$A_f = \pi \frac{{D_h}^2}{4} \tag{6}$$

Where D_h is the inside tube's diameter.

The formula described here is used for determining the PV panel's electric effectiveness:

$$\eta_{el} = \frac{E_p}{E_{in}} \tag{7}$$

The instantaneous TE of the PVT-C is obtained using the following equation:

$$\eta_{th} = \frac{E_{th}}{E_{in}} \tag{8}$$

Instantaneous TE can also be expressed as follows [33,35]:

$$\eta_{th} = \eta_0 - a_1\frac{T_m - T_a}{G} - a_2 G\left(\frac{T_m - T_a}{G}\right)^2 \tag{9}$$

η_0 is the optical efficiency and represents the collector efficiency at $T_m = T_a$, while a_1 and a_2 represent the linear and quadratic heat loss coefficients of the collector, T_m is the average fluid temperature, calculated by combining the temperatures at the collector's input and outflow.

The OE of the PVT-C is obtained using the following expression:

$$\eta_g = \frac{E_{th} + E_p}{E_{in}} \tag{10}$$

The Reynolds number is calculated in the heat exchanger to determine whether the fluid is in a laminar or turbulent domain, as shown below:

$$R_e = \frac{u_{in}D_h}{\nu} \tag{11}$$

2.2.2. Basic equations

During the building of the numerical model to assess the temperature distribution in the PVT-C, a couple of conditions are considered under consideration:

(1) The system is considered to be in a steady state.
(2) The flow of the fluid through the heat exchanger was completely uniform, laminar, and incompressible.
(3) No dust accumulates on the surface, affecting the absorptivity of the PVT-C,
(4) It is assumed that ethyl vinyl acetate (EVA) is perfectly transparent and transmits light,
(5) All thermal and fluidic properties are considered constant, regardless of temperature variations,
(6) There is no heat transfer occurring from the edges and the underside of the PVT-C.

Heat transfer within the solid parts of the PVT-C, including elements such as glass, EVA, PV cell, Tedlar, and heat exchanger, was mainly considered as a thermal conduction process. In this mechanism, the thermal energy propagates through the material through the vibratory movements of the particles. The resolution of the heat transmission through the surface of the PV cells is based on the use of the following thermal conduction equation [17,36]:

$$\frac{\partial^2 T}{\partial x^2} + \frac{\partial^2 T}{\partial y^2} + \frac{\partial^2 T}{\partial z^2} = 0 \tag{12}$$

The following equations, solved numerically with COMSOL, include the continuity equation and the conservation of momentum equations [17,36]:

$$\frac{\partial u}{\partial x} + \frac{\partial v}{\partial y} + \frac{\partial w}{\partial z} = 0 \tag{13}$$

$$\left.\begin{aligned} u\frac{\partial u}{\partial x} + v\frac{\partial u}{\partial y} + w\frac{\partial u}{\partial z} &= -\frac{1}{\rho}\frac{\partial p}{\partial x} + \nu\left[\frac{\partial^2 u}{\partial x^2} + \frac{\partial^2 u}{\partial y^2} + \frac{\partial^2 u}{\partial z^2}\right] \\ u\frac{\partial v}{\partial x} + v\frac{\partial v}{\partial y} + w\frac{\partial v}{\partial z} &= -\frac{1}{\rho}\frac{\partial p}{\partial y} + \nu\left[\frac{\partial^2 v}{\partial x^2} + \frac{\partial^2 v}{\partial y^2} + \frac{\partial^2 v}{\partial z^2}\right] \\ u\frac{\partial w}{\partial x} + v\frac{\partial w}{\partial y} + w\frac{\partial w}{\partial z} &= -\frac{1}{\rho}\frac{\partial p}{\partial z} + \nu\left[\frac{\partial^2 w}{\partial x^2} + \frac{\partial^2 w}{\partial y^2} + \frac{\partial^2 w}{\partial z^2}\right] \end{aligned}\right\} \tag{14}$$

Within the channels of the PVT-C exchanger, conjugated heat transfer is the predominant phenomenon, and it can be formulated as follows [17, 36]:

$$u\frac{\partial T}{\partial x} + v\frac{\partial T}{\partial y} + w\frac{\partial T}{\partial z} = -\frac{1}{\rho}\frac{\partial p}{\partial x} + k\frac{1}{\rho \times C_p}\nu\left[\frac{\partial^2 T}{\partial x^2} + \frac{\partial^2 T}{\partial y^2} + \frac{\partial^2 T}{\partial z^2}\right] \tag{15}$$

2.2.3. Boundary conditions

√Following equations articulate the boundary conditions to the upper surface of the PVT:

•A heat flow directed towards the interior: $-k_g\frac{\partial T_g}{\partial z} = G$

•A diffuse surface condition: $-n.q = \varepsilon_g\sigma\left(T_s{}^4 - T_g{}^4\right)$ where $\sigma\left(= 5,670367 \times 10^{-8} Wm^{-2}K^{-4}\right)$ is the constant of Stefan-Boltzmann.

•There is convection heat loss: $-n.q = h_{g-a}\left(T_a - T_g\right)$

√For the interfaces between the solid and fluid ducts, in particular at the interface between the water and the heat exchanger, the boundary condition is as follows:

•At solid-fluid interface: $\left(\frac{\partial T_s}{\partial n}\right)_{fluid} = \frac{k_s}{k_w}\left(\frac{\partial T_s}{\partial n}\right)_{solid}$

√ At all solid limits of the fluid passage line: no-smoothing condition:

•$u = v = w = 0$

√ The conditions at the heat exchanger inlet limits were specified in terms of velocity and inlet temperature, while the conditions at the heat exchanger outlet limits were set at zero pressure. There are expressed by:

•At the inlet: $T = T_{in}, u = U_{in}, v = w = 0$

•At the outlet: $P = 0$

√The other limits of the PVT-C are isolated:

$$\frac{\partial T_s}{\partial n} = 0$$

2.3. Mesh generation

Once the limiting conditions of the computational model have been defined, the model mesh is generated to solve the linear algebraic equations. In COMSOL, PVT and PV modules are meshed using a physics-controlled meshing sequence. This approach results in a progressive increase in the number of grids elements at each limit, enabling precise resolution of heat transfer phenomena and flow fields. At a volume FR of 180 L/h, an ambient temperature of 298.15 °C and G of 10^3 W/m^2, an independent mesh verification was carried out for the PVT-C. For PV and PVT-C, different nonuniform grid configurations are

examined, as specified in Table 3. The control parameter taken into consideration is the solar CT. There is no significant variation in solar CT from mesh 58,493 for the PV system. However, for the PVT-C, we opt for the smallest temperature difference between the two consecutive grids, which occurs between meshes 5,791,537 and 21,637,513. In other terms, the mesh count of 5,791,537 proved sufficient to ensure calculation accuracy. Consequently, for this numerical analysis, we have selected the PV and PVT-C models, consisting of 176,166 and 5791,537 elements respectively. Figs. 3(a) and (b) present the meshes of the PV and PVT-Cs, providing a visual representation of their configuration.

2.4. Model validation

The present simulation's correctness has been established by the use of two validation methods: firstly, employing a 3D numerical model for the PVT-C, and secondly, by comparing the results with experimental data.

2.4.1. Validity of experimental results

Solar cell temperatures were simulated under irradiation of 995 W/m^2 for different flow values (60, 90 and 180 L/h) using our current numerical model. The validity of this model was confirmed by comparing it with that developed by Rahman et al. [29]. The study carried out by Rahman et al. [29] was based on a SY-90 M PV module with dimensions of 1200 * 545 * 35 mm, comprising monocrystalline cells arranged in a 4 × 9 configuration. A rectangular heat exchanger with dimensions measuring 950 * 420 mm was utilized, consisting of 7 copper tubes, each with a diameter of 2.2 cm. The heat exchanger inlet conditions are a temperature of 35 °C, while the ambient temperature is 27 °C. Table 4 demonstrates a high level of consistency among the experimental data and the simulation's findings.

2.4.2. Validity of numerical results

Temperature validation of the numerical results involved a comparison in both the flow channel and at the outermost layer of the PVT-C designed according to Nahar et al. [4], with those determined by the same team. The following parameter were applied in the numerical simulation such as the solar radiation (10^3 W/m^2), and the ambient and input temperature are 34 °C and 34 °C, respectively and the values of the flow velocity is 0.0007 m/s in the inlet. These values correspond to those reported in the Nahar et al. [4]. Fig. 4 depicts an examination of the temperature's gradient within the flow channel and the PVT-C's temperature surface gradient. In the simulation of Nahar et al. [4], the flow channel temperature varied from 34 to 60.12 °C, whereas in the current simulation, this range is from 34 to 60.3 °C. With regard to surface temperature, in the simulation of Nahar et al. [4], is between 33.994 °C and 125.68 °C, whereas in the current simulation it was between 34 °C and 126 °C. It is therefore clear that the results obtained are in concordance with those obtained in [4].

3. Results and discussion

We conducted a numerical analysis in three dimensions to assess a new PVT-C's performance in relation to different parameters, such as volume FRs and irradiance levels. These parameters can vary between 30 and 210 L/h for volume FR and between 2 × 10^2 and 10^3 W/m^2 for solar irradiation. The ambient temperature is configured at 25 °C, with the inlet temperature established at 29 °C. The ensuing sections provide specifics on the outcomes for every scenario.

3.1. Effect of irradiation

The variations in wind speed, ambient temperature, incident solar irradiation, and, on the other hand, the artificial cooling process that the system is subjected to are the key factors influencing the evolution of the temperatures of the various constituent elements of the PVT-C. The surface temperature distribution of the uncooled PV module is displayed in Figs. 5(a)–(e) for solar irradiation levels between 2 × 10^2–10^3 W/m^2, as determined by the three-dimensional numerical analysis that was carried out. The front surface of the PV module achieves temperatures within the range of 39 °C to 94.4 °C, representing the minimum and maximum values, respectively. In addition, lower temperatures are observed along the edges of the module due to significant convection heat exchanges with the environment in three different directions. However, in the center of the PV module, the elevated temperatures observed can be attributed to the limited convective heat transfer to the environment, occurring in only two directions. (towards the glass layer and the Tedlar layer), resulting in significant heat accumulation. Fig. 5 (f) shows a real thermal image, captured by an infrared camera, which confirms the temperature distribution obtained by the numerical analysis.

Figs. 6(a)-(j) illustrate the impact of G on the surface temperature of the PVT-C and the temperature of the water inside the heat exchanger. The temperature distribution is shown for irradiation varying from 2 × 10^2 to 10^3 W/m^2, with a fixed water inlet temperature of 29 °C and a volume FR of 180 L/h. As can be seen in figures (a)-(e), the highest temperature of the PVT-C decreases significantly from 46 to 32.1 °C when G goes from 10^3 to 2 × 10^2 W/m^2. This is because when irradiation is high, a large quantity of energy is absorbed by the PVT-C, resulting in greater heat production. This accumulation of heat in the PVT-C causes an increase in the internal temperature of the photovoltaic cells.

The temperature variations of the heat transfer fluid (water) circulating in the heat exchanger, for different values of solar irradiance at a volumetric FR of 180 L/h, are illustrated in Figs. 6(f) to 6(j). At low solar irradiance levels, the fluid temperature at the collector outlet is generally low and increases as solar irradiance levels rise. This is due to the increased accumulation of heat by the cooling fluid through the PVT-C's heat exchanger at higher solar irradiance. These figures highlight a significant change in the temperature distribution of the fluid around the inlet and outlet ports for higher irradiance levels. The average fluid temperature at the collector inlet is maintained at 29 °C. At an irradiance of 2 × 10^2 W/m^2, the cooling fluid temperature varies from 29 °C to 31.5 °C. This variation extends from 29 °C to 42.7 °C for an irradiance of 10^3 W/m^2.

3.2. Effect of flow rate

Fig. 7 illustrates how the FR affects the PVT-C surface temperature

Table 3
Verification of grid sensitivity.

PV	Type of meshing	Coarser	Coarse	Normal	Fine	Finer
	Elements	14,583	26,665	58,493	176,166	1,074,080
	Cell temperature (°C)	91.79	91.73	91.72	91.72	91.72
	Time of solution (s)	4	8	14	43	259
PVT-C	Type of meshing	Coarser	Coarse	Normal	Fine	Finer
	Elements	2,130,848	2,558,407	3,139,697	5,791,537	21,637,513
	Cell temperature (°C)	34.24	34.65	35.10	34.11	34.50
	Time of solution (s)	1659	2324	3412	8987	12,875

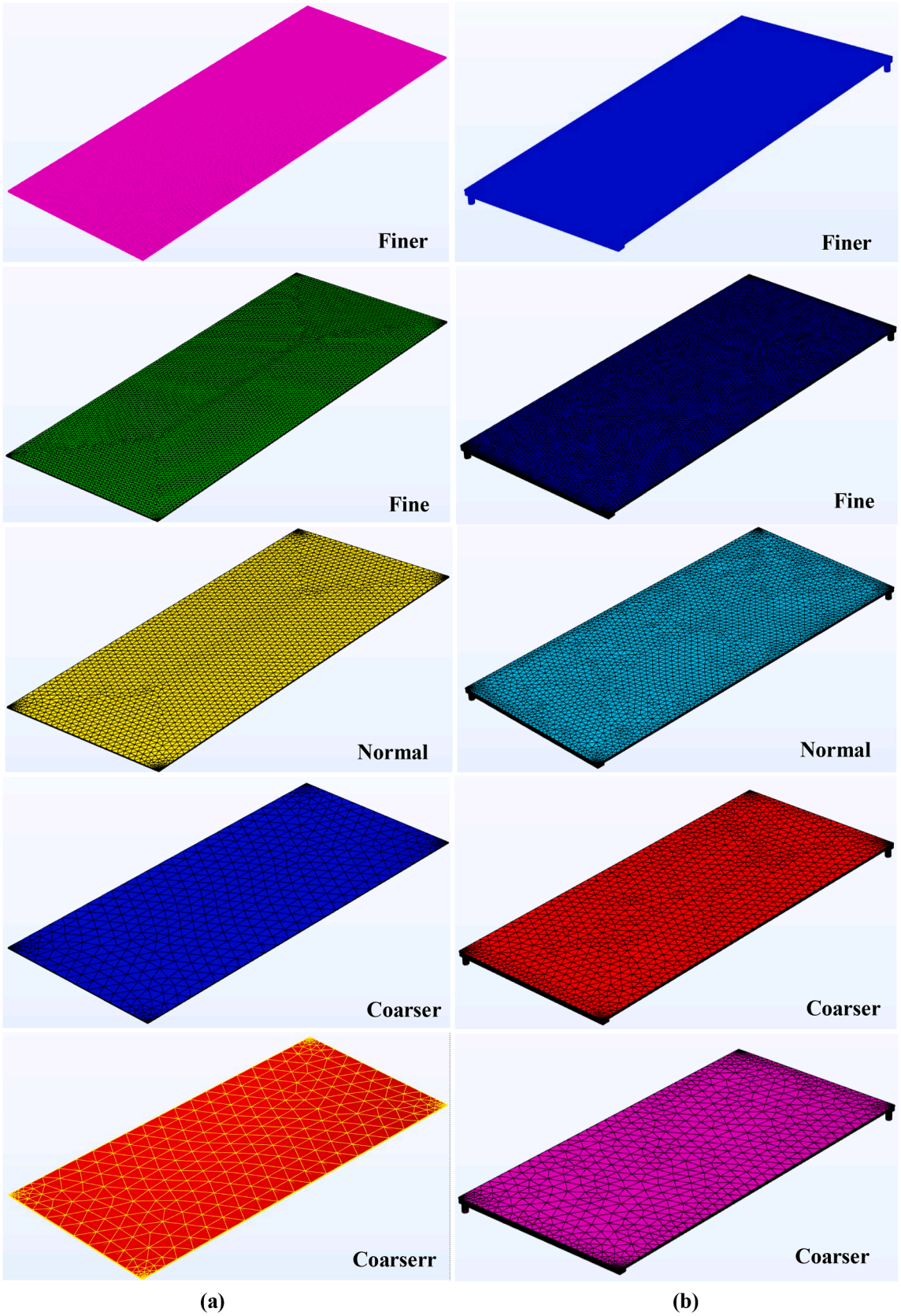

Fig. 3. Various meshing configurations applied to PV (a) and PVT-Cs (b).

Table 4
Model validation of solar CT of PVT against FR.

volumetric FR (L/h)	T_{sc} (°C)		Error percentage (%)
	Current research	Rahman et al [29]	
60	52.44	50.23	4.21 %
90	49.54	49.65	0.22 %
180	46.11	47.76	3.45 %

when it is exposed to 10^3 W/m^2 of solar radiation. These figures show that increasing the volumetric FR accelerates heat exchange across the surface of the heat exchanger, thus promoting heat transfer to the heat transfer fluid. As the FR increases, the temperature differences along the collector surface decrease and the temperature distribution becomes relatively more homogeneous. This observation suggests that the variation in FR has a remarkable influence on the heat transfer rate between the fluid and the surface of the exchanger. By varying the FR from 30 to 210 L/h, we observe that the maximum temperature difference along the surface of the collector goes from 48.2 °C to 15.9 °C. It should be noted that increasing the FR of the inlet fluid causes a progressive reduction in the maximum temperature at the level of the PVT-C. For a minimum FR of 30 L/h, the maximum temperature reached by the collector surface is 77.2 °C (Fig. 7(a)), while at a maximum FR of 210 L/h, the maximum temperature has decreased to 44.9 °C (Fig. 7(e)).

3.3. Solar cell PV temperature

The main aim of this work is to control the temperature of the PV panel (T_{sc}) near an average temperature and minimize temperature variations on the PV cell surface by using a suitable cooling system. Significant temperature changes can, in fact, harm semiconductor materials, which may have an effect on the efficiency and robustness of PV cells. Based on the current three-dimensional numerical analysis, Figs. 8(a) and 8(b) demonstrate the rise of T_{sc} in relation to the irradiation and the heat transfer fluid FR, respectively. Based on the available data, T_{sc} rises by roughly 0.7 °C for each additional 10^2 W/m^2 of irradiation. These results are comparable with those obtained in similar studies carried out by Bahaidarah et al. [37], Nasrin et al. [31], Teo et al. [38], Rahman et al. [29], Chandrasekar et al. [39], as well as Nasrin et al. [33]. They found that increasing the irradiance level in the presence of the cooling system was associated with elevations in cellular temperature. Table 5 presents a comparison of the increment per 10^2 W/m^2 of the PV cells temperature obtained in the present study and different studies reported in the literature. A very good deal was noted between the current result and that obtained by Nasrin et al. [33]. However, the result obtained is slightly different from those of Bahaidarah et al. [37], Nasrin et al. [31], Teo et al. [38], Rahman et al. [29] and Chandrasekar et al. [39] due to differences in solar irradiance variation range, the physical characteristics of each PVT-C, wind speed, ambient temperature, and the module's operating temperature variation range.

As the fluid FR rises, the average of T_{sc} decreases at $G = 10^3$ W/m^2 and T_{in} value of 29 °C, as illustrated in Fig. 8(b). Indeed, when the FR of the inlet fluid increases, the amount of heat removed from the module by convection also increases, which results in a diminution in the average of T_{sc}. For a FR of 30 L/h, the average of T_{sc} obtained is 55.47 °C. This temperature gradually decreases to 40.07 °C when the FR reaches the value of 180 L/h. At a FR of 210 L/h, T_{sc} decreases by 0.54 °C compared to that obtained for a FR of 180 L/h, but this is accompanied by an increase in pumping power. Thus, for the PVT-C considered, it is possible to note that the optimal volumetric FR of the cooling fluid is 180 L/h.

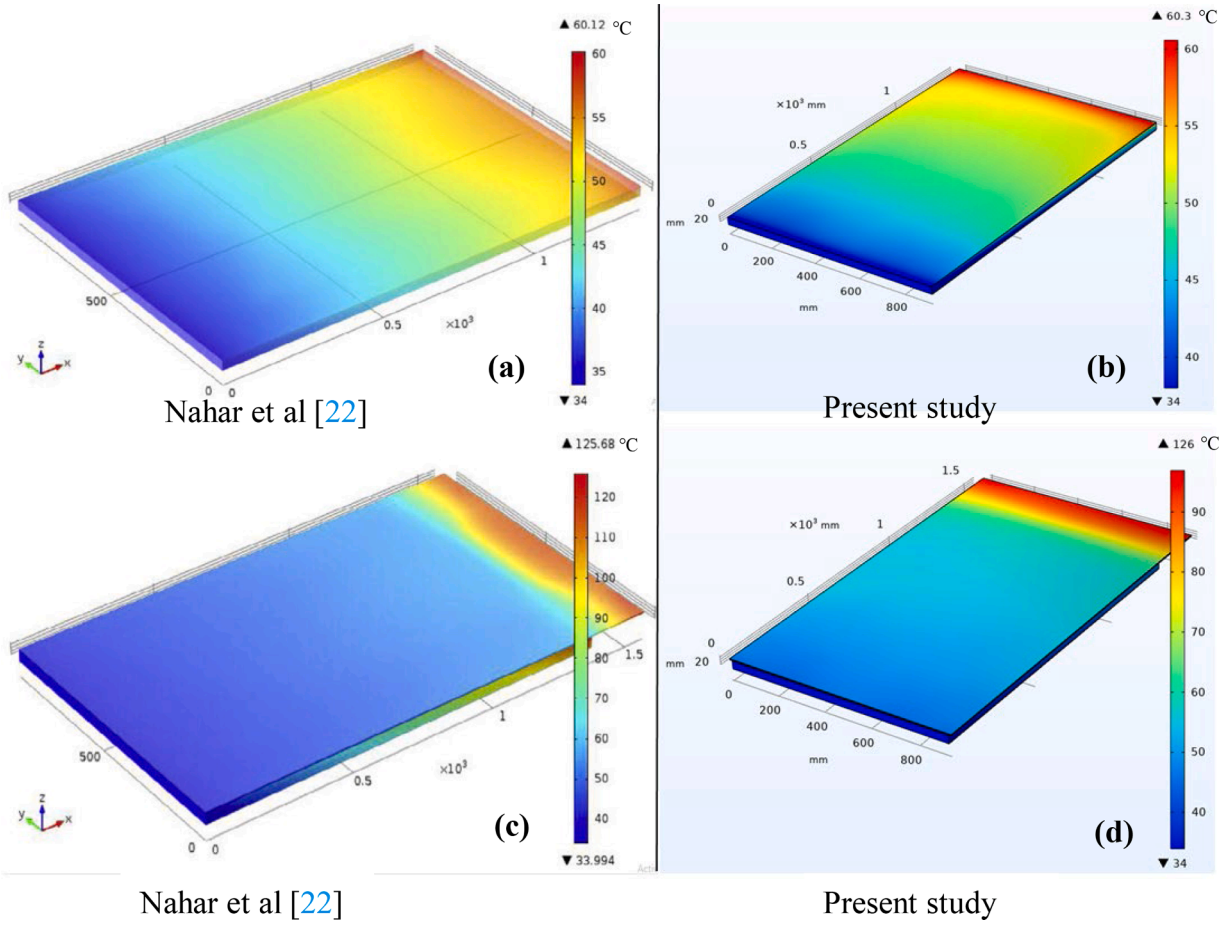

Fig. 4. Model validation of the flow channel (a-b) and PVT-C surface temperature graph (c-d).

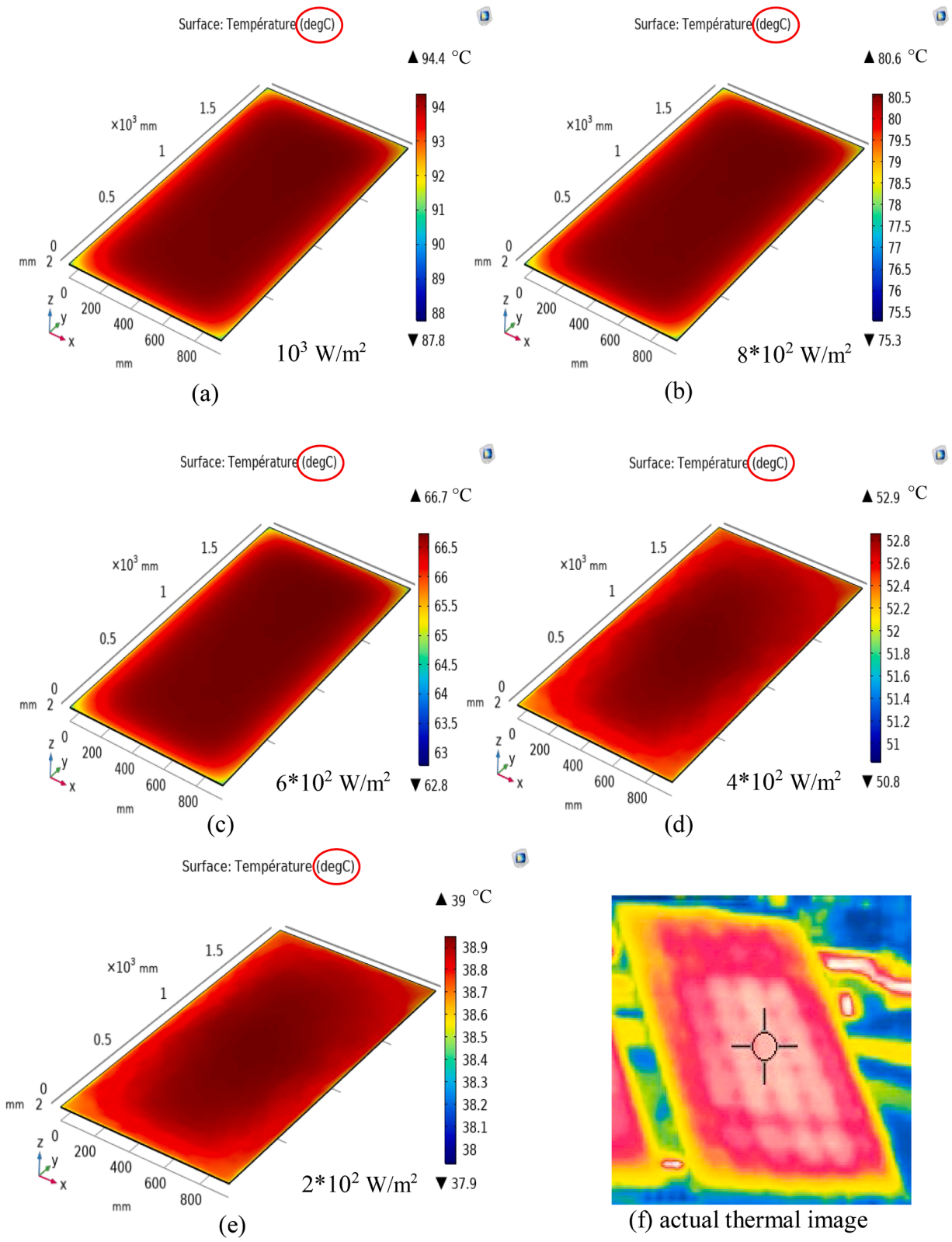

Fig. 5. (a)-(e) PV panel temperature variation as a function of irradiation, (f) actual thermal image.

3.4. Study of electrical power evolution

Figs. 9(a) and (b) present the evolution of the electrical output power based on volume flow and solar irradiation, respectively. In particular, in Fig. 9(a), observing that, at an input temperature of 29 °C and FR of 180 L/h, the power generated by the PVT-C goes from 38.45 W below an irradiance level from 2×10^2 W/m^2 to 187.02 W under an irradiance level of 10^3 W/m^2, a rise of 18.57 W per 10^2 W/m^2. The present result is slightly different at the values 3.88 W and 6.4 W found, respectively, by Rahman et al. [29] and of Nasrin et al. [31]. These discrepancies could be attributed to a variety of variables, such as PV module size, fill factor, operating temperature, reference temperature, system cooling

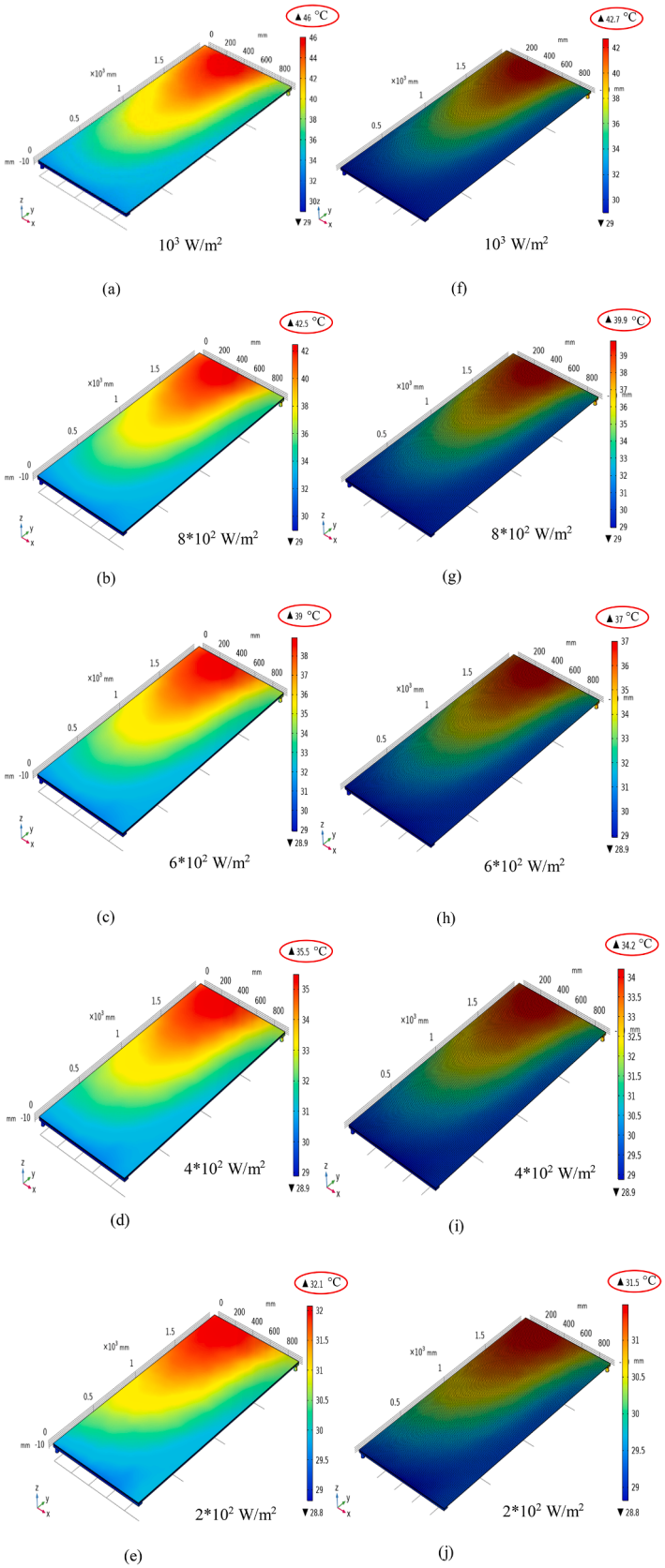

Fig. 6. Distributions of PVT-C surface temperature (a)-(e) and heat transfer fluid temperature (f)-(j) for different irradiation values.

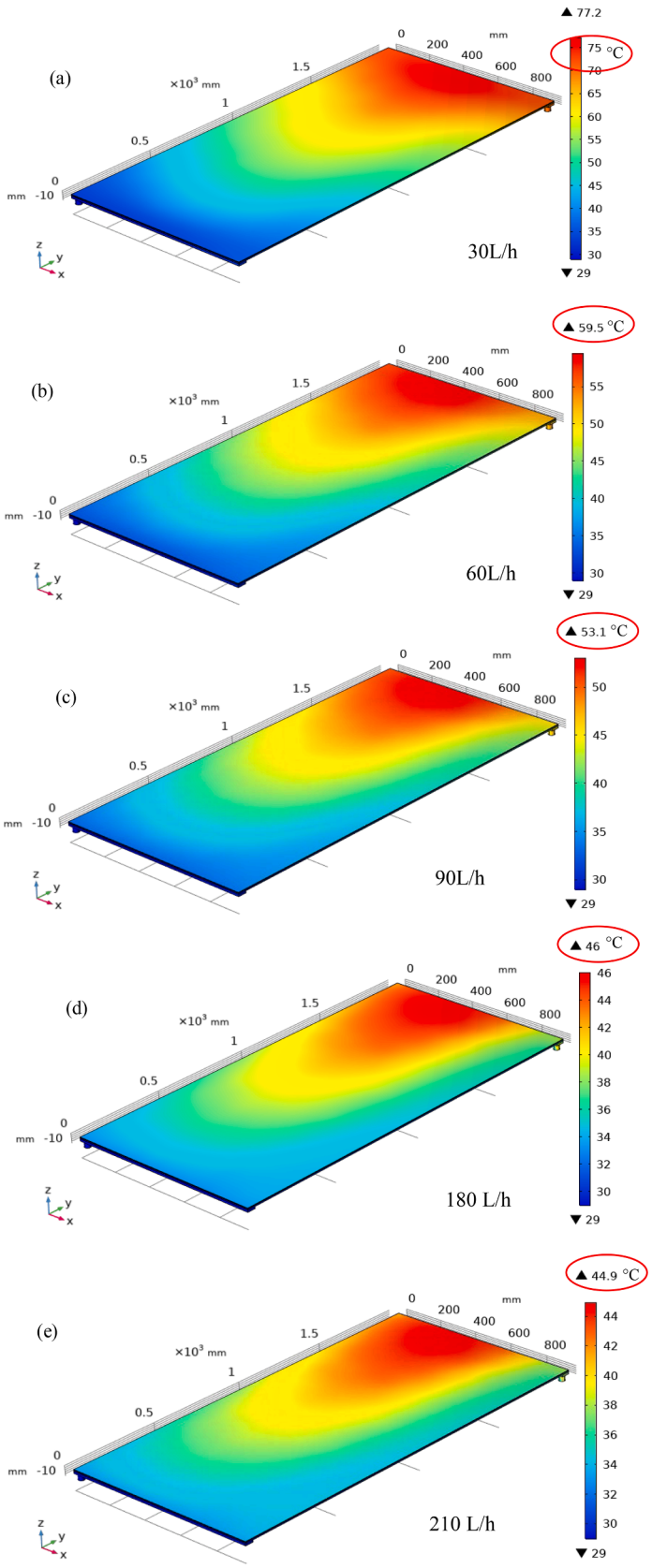

Fig. 7. Variation of PVT surface temperature for different FR's.

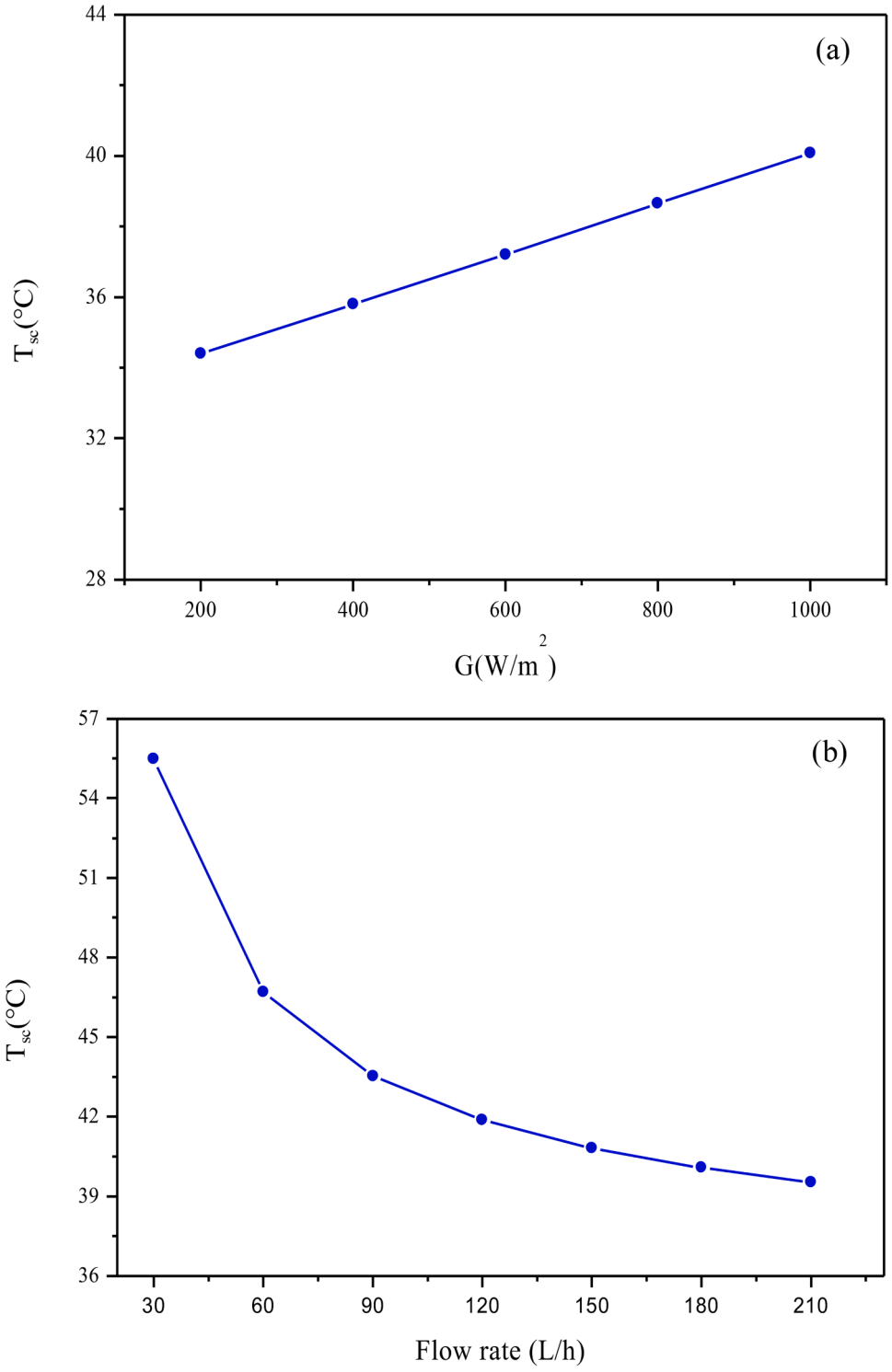

Fig. 8. Evolution T_{sc} as a function of irradiation (a) and FR (b).

configuration difficulties, and material properties.

Fig. 9(b) evaluates the effect of fluid volume FR on electrical power under constant irradiance of 10^3 W/m^2 and a T_{in} of 29 °C. The results show that the electrical power delivered for an initial FR of 30 L/h is 173.12 W. When 180 L/h of FR is reached, the output power rises to 187.02 W. However, it is essential to note that beyond this point, despite further increases in water FR up to 210 L/h, the power output did not experience significant variations and stabilized around 187.49 W. According to this study, the electrical power increases by 0.798 W per each 10 L/h increase in FR of heat transfer fluid.

3.5. Study of electrical efficiency

Figs. 10(a) and (b) illustrate the variation of the EE of the PVT-C depending on solar irradiance and volumetric FR over the ranges from 2×10^2 to 10^3 W/m^2 and from 30 to 180 L/ h, respectively. It should be pointed out that with the increase in irradiation, in particular for a T_{in} of 29 °C and a FR of 180 L/h, the EE of the PV module decreases by 12.45 %

Table 5
Comparison of the increase in temperature of PV cells per 10^2 W/m^2 of irradiance obtained in different studies.

Investigations	G (W/m^2)		T_{sc} (°C)		T_{sc} (°C) increment per 10^2 W/m^2	T_{amb} (°C)
	Starting	Ending	Starting	Ending		
Bahaidarah et al.[37]	240	979	21	35	1.9	21
Nasrin et al. [31]	1000	3000	48	85	1.85	32
Teo et al.[38]	550	1050	41	48	1.4	–
Chandrasekar et al.[39]	600	1300	40	50	1.4	37
Nasrin et al. [33]	1000	5000	43	78	0.9	32
Rahman et al.[29]	312	995	31	50	2.71	35
Present research	200	1000	34.40	40.07	0.7	25

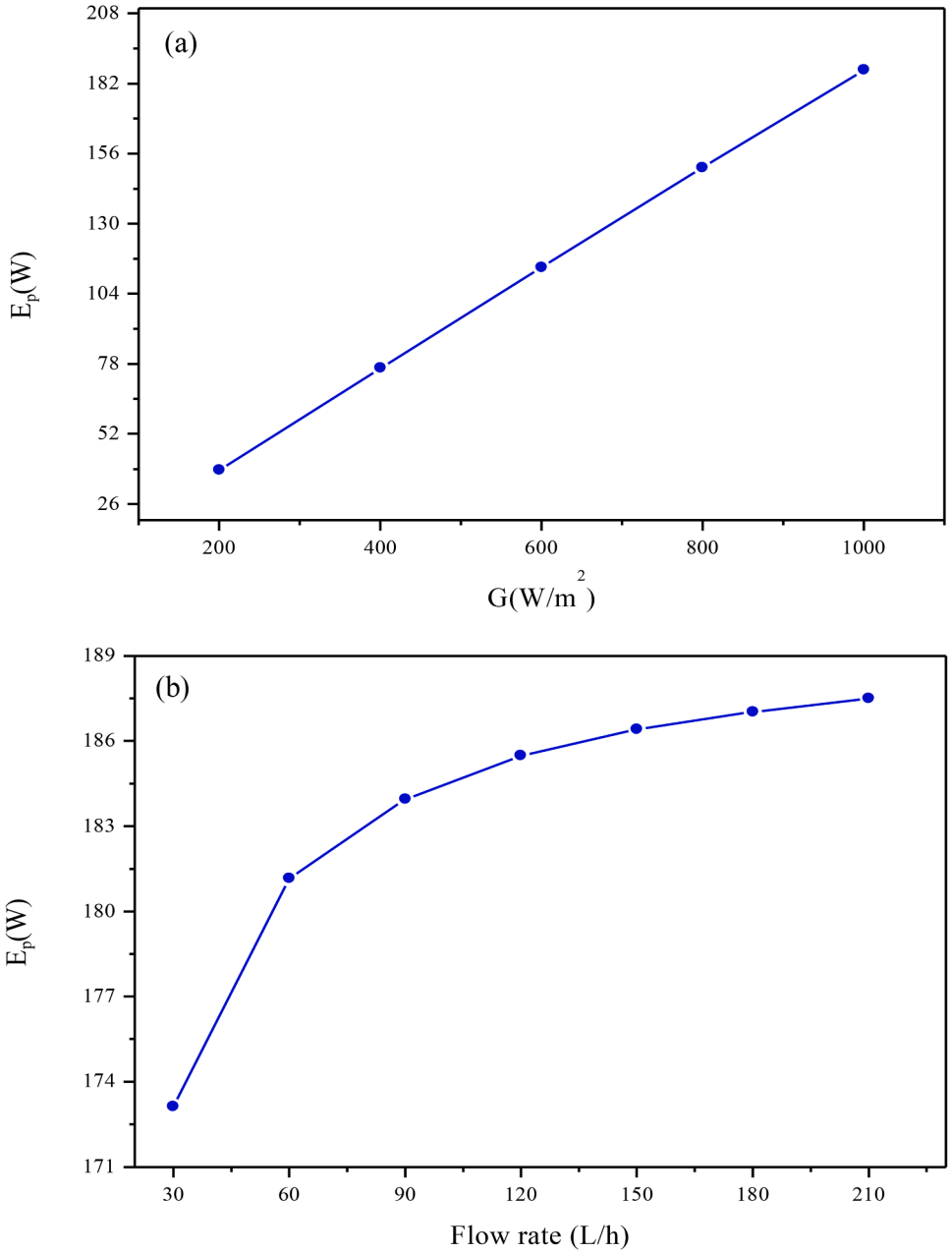

Fig. 9. Evolution of the electrical power with the irradiance (a) and with the FR (b).

at 12.11 % when the solar irradiance rises from 2×10^2 to 10^3 W/m^2. As a result, there is a decrease of approximately 0.04 % in EE per each 10^2 W/m^2 augmentation of irradiance. Studies by Rahman et al. [29], Nasrin et al. [31], Nahar et al. [4] and Nasrin et al. [33] also indicated that PV panel efficiency reduced by around 0.87, 0.09, 0.16 and 0.06 % for each 10^2 W/m^2 increase. Our system therefore outperforms previous studies.

The variation of the FR of inlet water has a positive effect on the EE of the PVT-C, as shown in Fig. 10(b). Over a range of 30 L/h to 120 L/h of

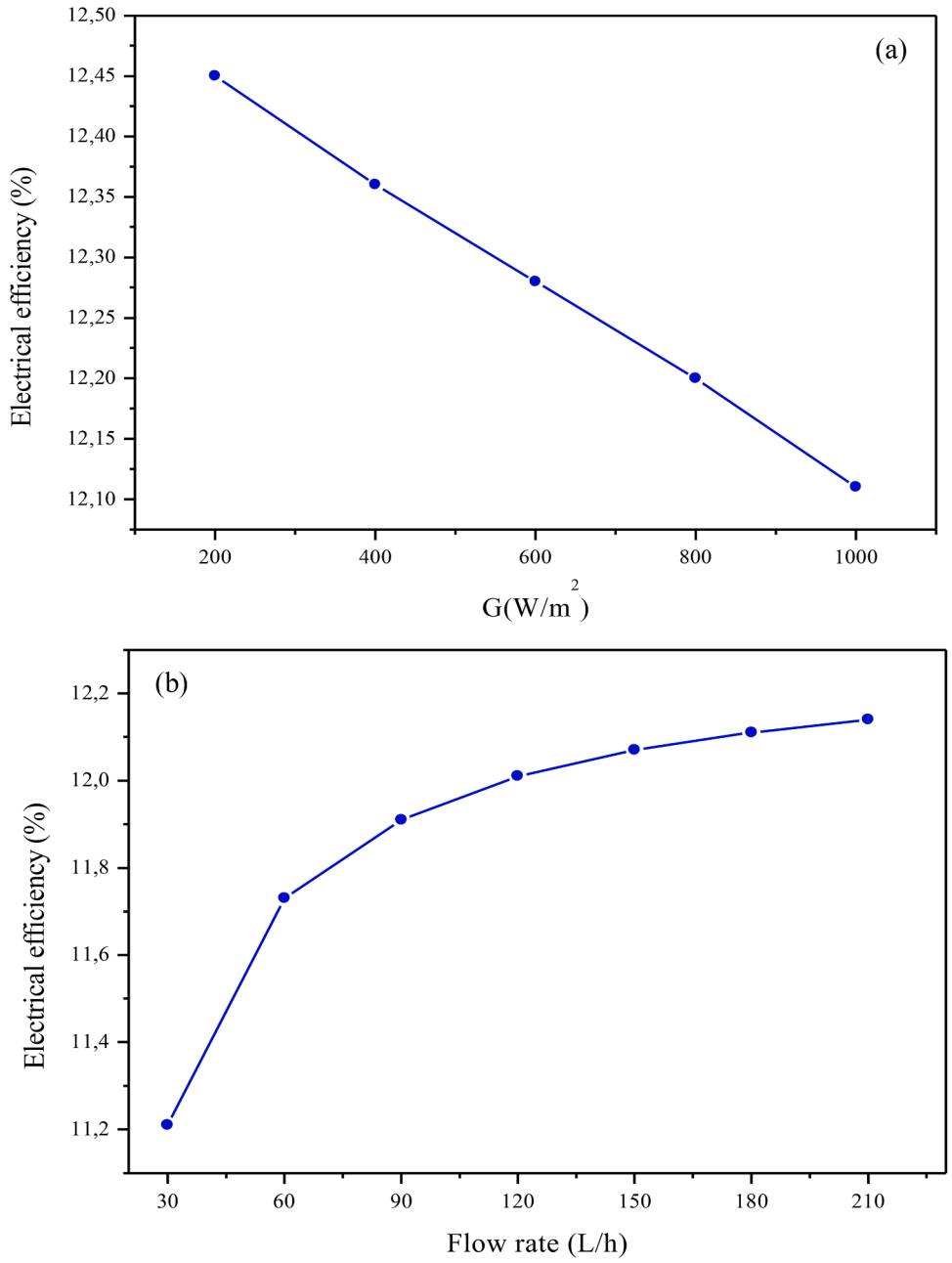

Fig. 10. Evolution of EE depending on solar irradiance (a) and FR (b).

volume FR, the efficiency increases from approximately 11.2 to 12.1 %. In fact, increasing the FR leads to a reduction in the operating temperature. It is worth noting that the output voltage of the PV module increases significantly with the reduction of T_{sc}. This increase in voltage contributes to a notable increase in EE. However, it is interesting to note that beyond a FR of 180 L/h, there is no significant improvement in EE. In other words, for the PVT-C cooling system, it is more advantageous to maintain the inlet water FR above 180 L/h.

3.6. Coolant outlet temperature

Figs. 11(a) and 11(b) depict variations in the average of T_{out} depending on G and volumetric FR. It can be observed that the rise in solar irradiance has a positive effect on the fluid temperature at the system outlet. When the volumetric FR and the water temperature at the inlet are kept constant at 180 L/h and 29 °C, respectively, the obtained fluid temperature at the outlet is approximately 30.04 °C for an irradiance of 2×10^2 W/m^2. However, this temperature increases to 34.78 °C when the irradiance reaches 10^3 W/m^2. Thus, T_{out} increases by approximately 0.6 °C for every 10^2 W/m^2 increment in solar irradiance.

On the contrary, for a T_{in} of 29 °C and a FR of 180 L/h, the water outlet temperature decreases as the inlet FR increases, as illustrated in Fig. 11(b). This downward trend can be attributed to the increase in the heat transfer rate by convection resulting from rising fluid velocity. With a rise in flow velocity, the heat dissipation rate also increases, allowing less time for heat accumulation, resulting in a decrease in T_{out}.

3.7. Thermal energy

Fig. 12 illustrates the dependence of thermal energy according to the of irradiance over a range of 2×10^2 to 10^3 W/m^2. For a FR of 180 L/h and under an irradiance of 2×10^2 W/m^2, the accumulated thermal energy is 218.4 W. This value increases significantly, reaching 1213.8 W for $G = 10^3$ W/m^2. This significant increase in thermal energy can be

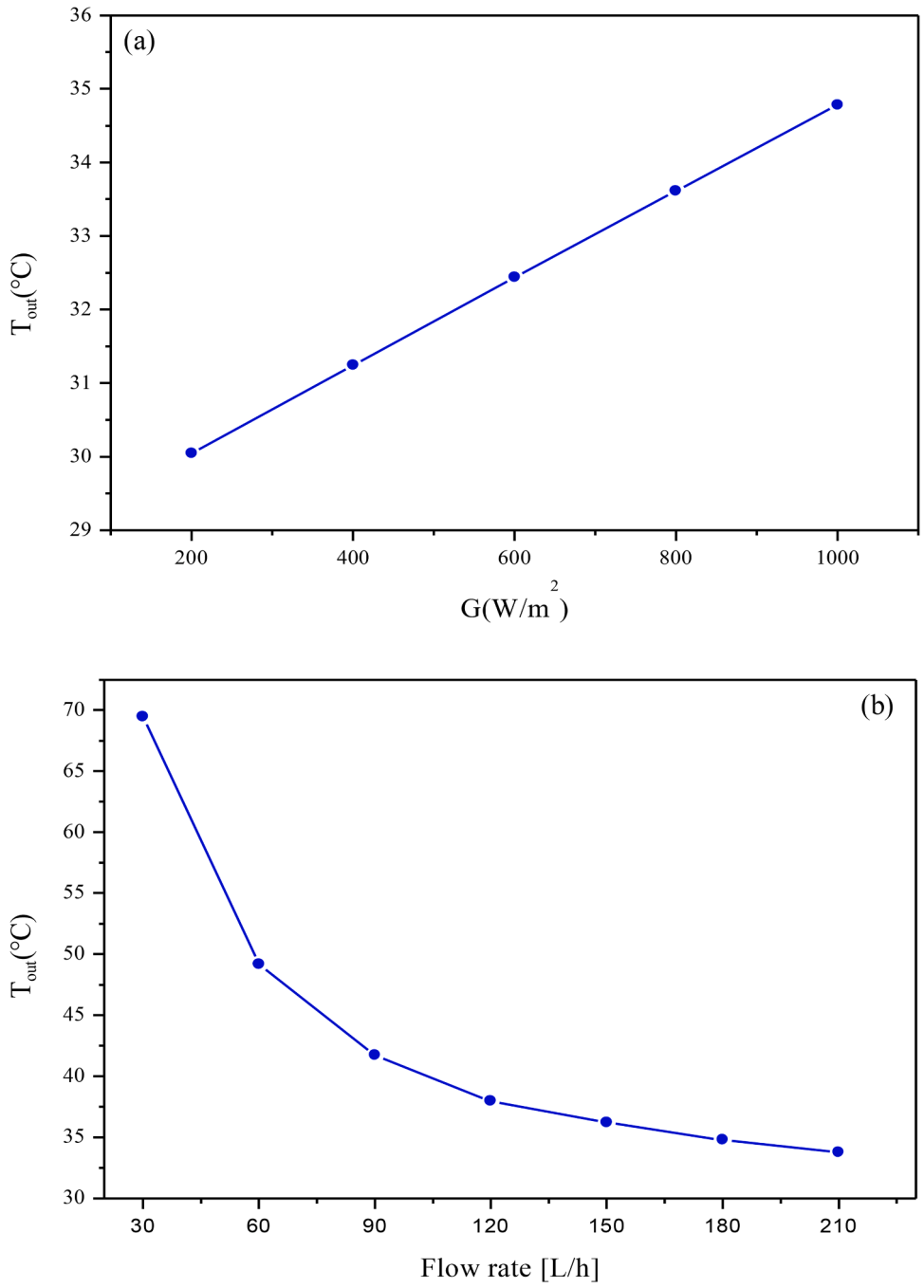

Fig. 11. Variation of the outlet temperature with relation to irradiance (a) and to FR (b).

explained by the heat transfer by conduction through the surfaces of the different layers constituting the PVT-C and the heat transfer by convective inside the circulating fluid. Due to the high irradiance, this results in a significant difference between fluid temperatures at the inlet and outlet of the exchanger. Thus, thermal energy rises by 124.42 W per each 10^2 W/m^2 increase in irradiance. Additionally, there are several additional applications for this large quantity of thermal energy, including cleaning, bathing, and structure heating.

3.8. Thermal efficiency

Fig. 13 illustrates the variation of TE depending on solar irradiance, which varies from 2×10^2 to 10^3 W/m^2. This variation is observed by maintaining a constant a T_{in} of 29 °C and a FR of 180 L/h. It is apparent that the TE increases with solar irradiance, reaching its maximum at 10^3 W/m^2, with a value of 78.59 %. Furthermore, it is noteworthy that a 10^2 W/m^2 increase in solar irradiance results in approximately an 0.98 % increase in TE. This increase is attributed to an increase in the rate of heat transfer by conduction through the layers of the PV module and between the Tedlar layer and the aluminum metal heat exchanger, as well as by convection between the surface of the exchanger and the coolant. Indeed, when the solar irradiance increases, a greater quantity of thermal energy is transmitted to the heat-transfer fluid, which increases the TE of the PVT-C.

The results obtained through the current three-dimensional analysis are confronted to the relevant results reported in the literature. This comparison is presented in Table 6, where it is notable that the designed system achieves a maximum TE of 78.59 %. This was achieved by

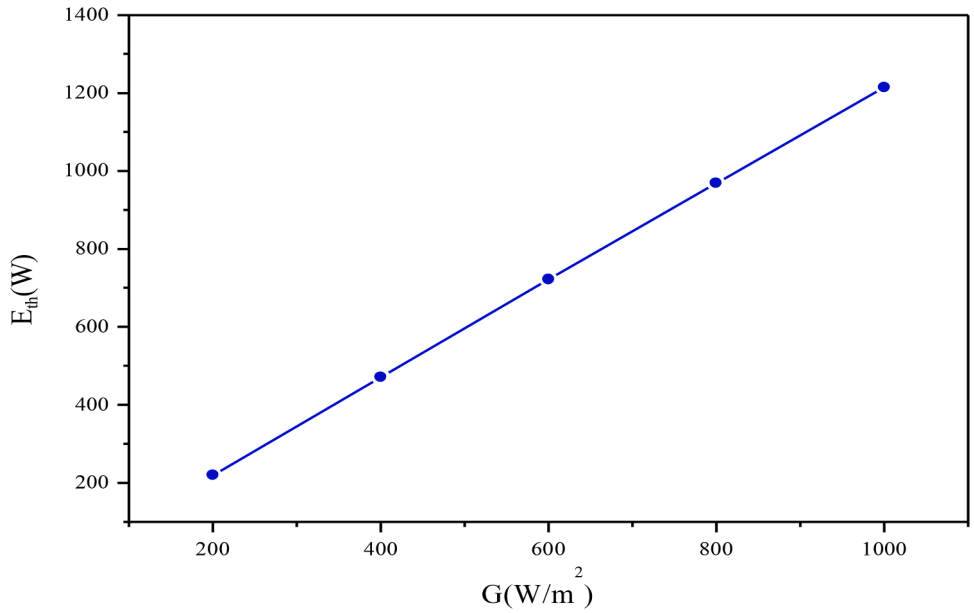

Fig. 12. Evolution of thermal energy depending on solar irradiance.

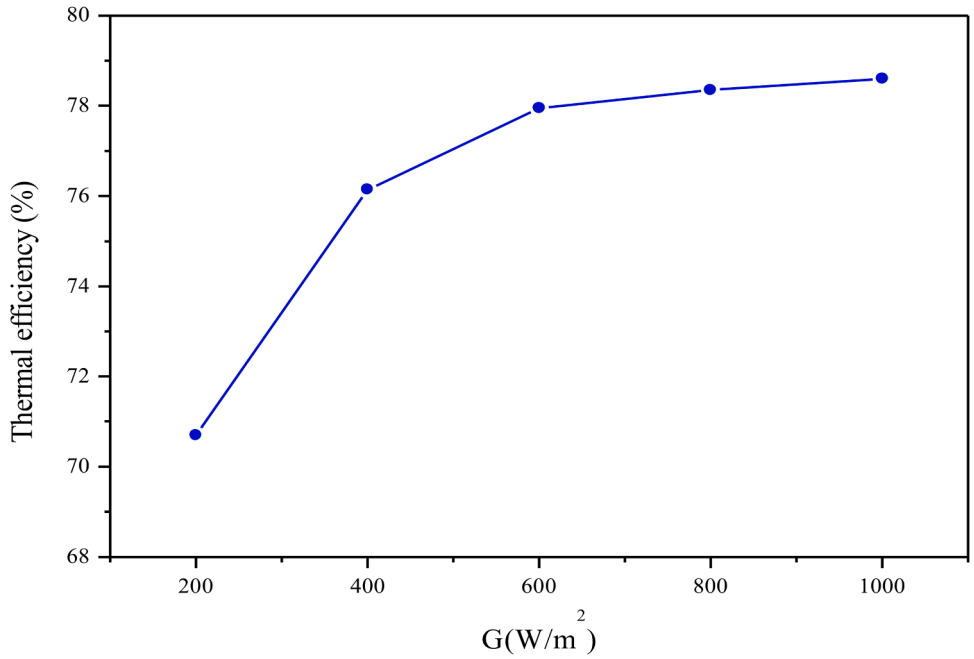

Fig. 13. Thermal efficiency variation according to irradiance.

maintaining a FR of 180 L/h and a T_{in} of 29 °C. Therefore, it is clear that the new cooling system developed in this study is significantly more efficient.

The evolution of the TE of the PVT-C depending on the reduced temperature (T*) is also analyzed. A regression of the results obtained by a quadratic equation (Eq. (9)) is used to describe the evolution of the TE (η_{th}) depending on T* (K m^2/W). The collector efficiency for $T_m = T_a$ (η_0) and the linear and quadratic heat loss coefficients a_1 and a_2 of the collector, as shown in Fig. 14, are obtained with a confidence coefficient of $R^2 = 0.956$. This result shows that the TE varies according to a quadratic

Table 6
Comparing results from this study with those from other studies reported in the literature.

Authors / Reference	Mass FR range (kg/s)	Irradiation Range (W/m^2)	Maximum TE (%)	Maximum EE (%)	Nature of study
Nahar et al. [4]	0.42–0.98	10^3	73	11.3	
Fayaz et al. [40]	0.006	2×10^2–10^3	76.1	13.74	Numerical using COMSOL
Fayaz et al. [40]	0.006–0.036	10^3	72	12.41	
Present study	0.05	10^3	78.59	12.11	

function of the reduced temperature for a volume FR of 180 L/h, as was suggested by Florschuetz [41]. it can be observed that when the reduced temperature is zero, the developed system achieves a maximum TE of 80.80 %. This represents a slight improvement of 4.6 % compared to the TE of 77.08 % obtained by Podder et al. [42].

Fig. 15 presents a comparison of the variation in TE as a function of reduced temperature, using regression through a linear expression, obtained in the current numerical study and that obtained by Yu et al. [43]. In the last study, the authors have evaluated the performances of two winding-linked PVT-Cs used in Chengdu, Sichuan, in western China, using both numerical and experimental methods. The absorber plate layouts of the two PVT-Cs were different; one had a traditional harp-channel arrangement, while the other had a unique grid-channel setup. Since a grid-channel PVT-C provides higher thermal and PV efficiency than a harp-channel PVT-C, that is how the comparison is made. Although the difference between the new design of the PVT-C and that presented by Yu et al. [35], the evolutions of thermal efficiency depending on reduced temperature are similar.

3.9. Overall efficiency

The evolution of the OE of the developed PVT-C depending on solar irradiance as illustrated in Fig. 16. When FR and inlet temperature are maintained at 180 L/h and 29 °C respectively, total system efficiency increases from 83.15 to 90.7 % as solar irradiance rises from 2×10^2 to 10^3 W/m^2. Consequently, for each increase of 10^2 W/m^2 in solar irradiance, there is a 0.94 % improvement in OE.

4. Conclusion

In this work, a new aluminum heat exchanger configuration, consisting of 94 channels and attached directly to the PV module, was designed, thus developing a new PVT-C. To analyze its behavior, numerical modeling was conducted by COMSOL software, built on the FEM. PV and PVT-C performance is analyzed depending on solar irradiance and volumetric FR. The temperature distribution within the PV and PVT-Cs is also described. In addition, various parameters are evaluated, including solar CT, coolant outlet temperature, electrical power generated and EE, thermal energy recovered and TE, as well as OE. The following essentially summarizes the study's main conclusions:

- An increase of 10^2 W/m^2 in incident solar irradiance on the PV system results in an increase of approximately 6.20 °C in T_{sc}, and an augmentation of approximately 12.92 W in the electrical power generated.
- A 10^2 W/m^2 increase in irradiance causes a 0.363 % drop in the PV system's EE.
- With every 10^2 W/m^2 rise in incident solar irradiance on the PVT-C, the CT, T_{out}, electrical power, thermal energy, TE, and OE increase approximately 0.7 °C, 0.6 °C, 18.57 W, 124.425 W, 0.98 % and 0.94 %, respectively.
- The EE of the PVT-C decreases by approximately 0.04 % for each augmentation of 10^2 W/m^2 in solar irradiance.
- For the PVT-C, every 10 L/h increase in fluid flow results in approximately 0.885 °C decrease in cell temperature, approximately 1.98 °C decrease in fluid temperature output, as well as an increase of approximately 0.798 W in the electrical power generated.
- The EE rises by about 0.051 % for each augmentation of 10 L/h in fluid flow.
- The optimum coolant FR for this collector when subjected to high solar irradiance of 10^3 W/m^2 is 180 L/h.

Finally, the proposed PVT-C offers good results in terms of temperature inhomogeneity and overall performance. In this context, it will be worthwhile recommending the realization of this new PVT-C, which is easy to integrate into the building and can be adapted to meet air or water needs according to the seasons and the building's thermal requirements.

Funding

This work did not receive any financial support.

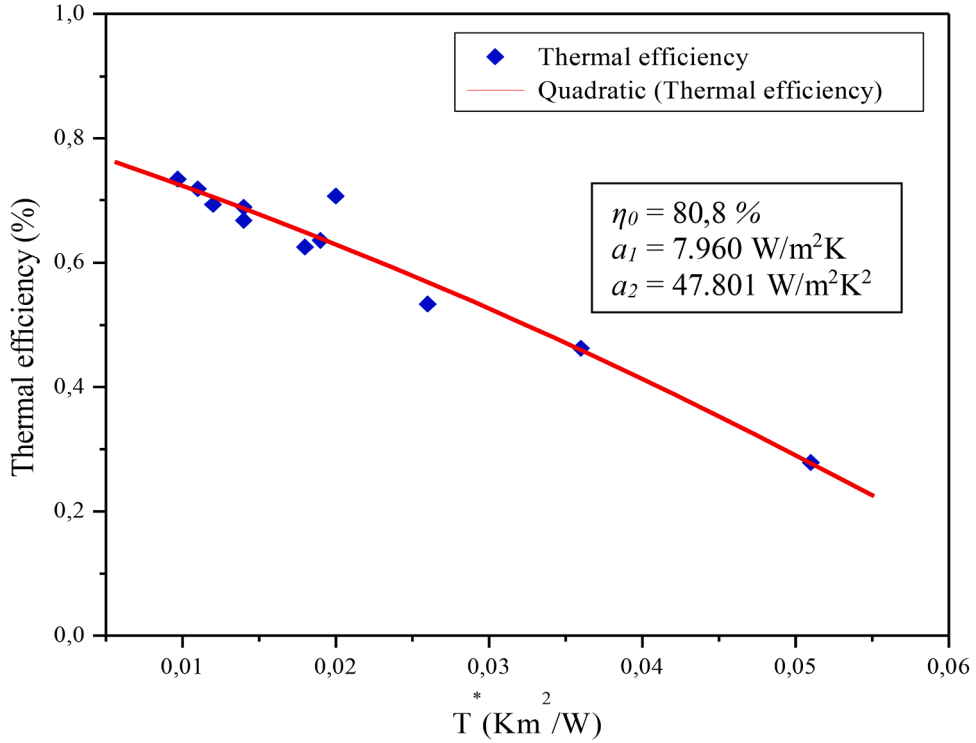

Fig. 14. Quadratic regression of the TE of the developed system according to the reduced temperature.

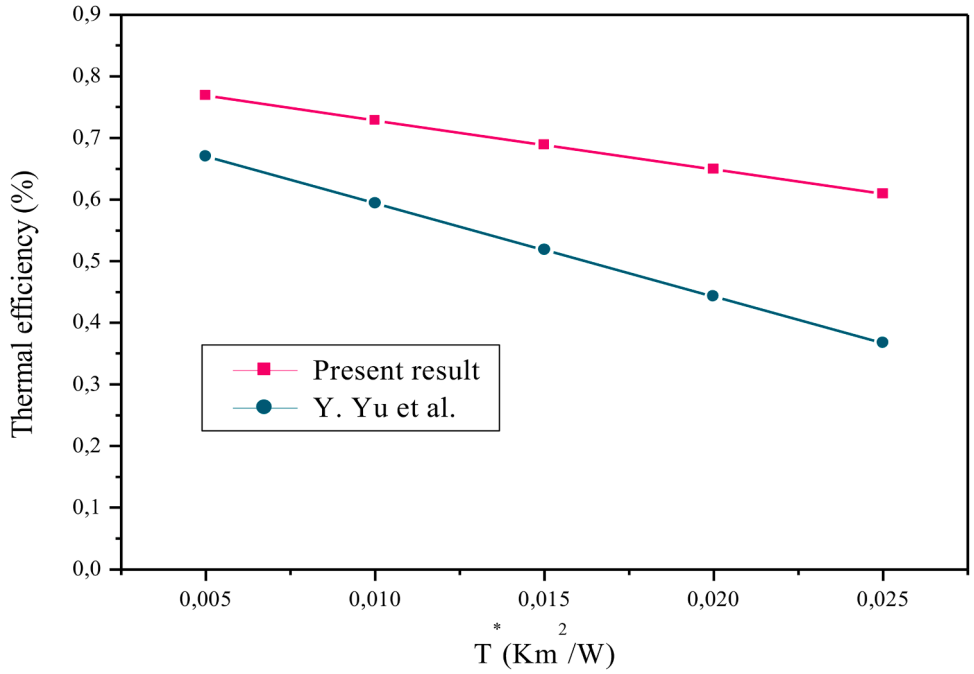

Fig. 15. Comparison of the linear regression results of the evolution of the TE according to reduced temperature with those obtained by Yu et al. [43].

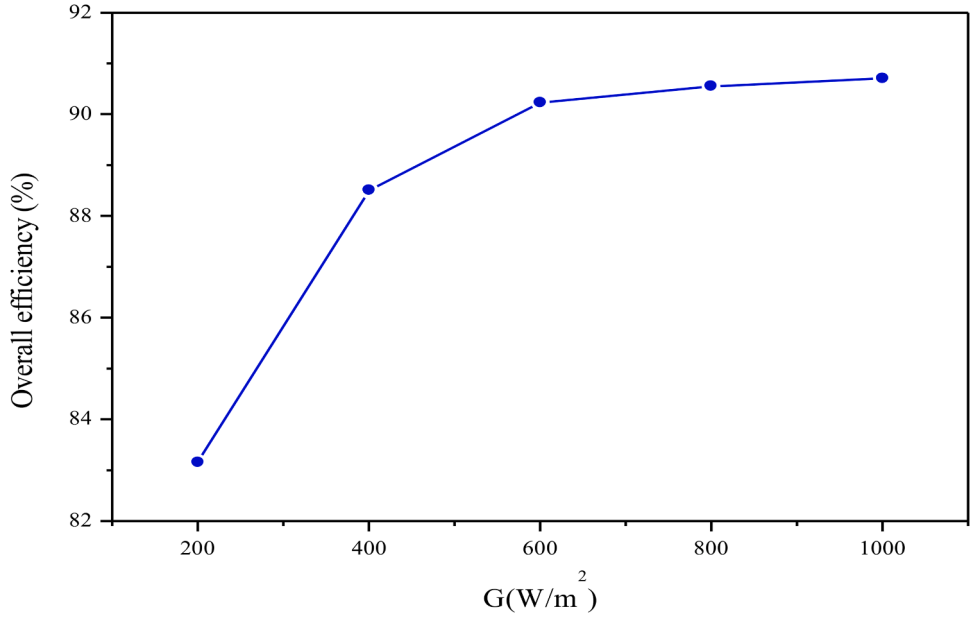

Fig. 16. Evolution of OE depending on of irradiance.

CRediT authorship contribution statement

Yassine El Alami: Writing – original draft, Visualization, Validation, Software, Methodology, Investigation, Funding acquisition, Formal analysis, Data curation, Conceptualization. **Ali Lamkaddem:** Writing – review & editing. **Rachid Bendaoud:** Writing – review & editing, Visualization, Validation, Supervision, Conceptualization. **Sofian Talbi:** Writing – review & editing. **Mohamed louzazni:** Writing – review & editing. **Elhadi Baghaz:** Writing – review & editing, Writing – original draft, Visualization, Validation, Supervision, Resources, Project administration, Methodology, Investigation, Funding acquisition, Formal analysis, Data curation, Conceptualization.

Declaration of competing interest

There are no conflicts to declare.

Data availability

No data was used for the research described in the article.

References

[1] R. Gupta, A.K. Yadav, S. Jha, P.K. Pathak, Time series forecasting of solar power generation using Facebook prophet and XG boost, in: 2022 IEEE Delhi Section

Conference (DELCON), New Delhi, India, 2022, pp. 1–5, https://doi.org/10.1109/DELCON54057.2022.9752916 n.d.
[2] P. Jha, B. Das, R. Gupta, J.D. Mondol, M.A. Ehyaei, Review of recent research on photovoltaic thermal solar collectors, Solar Energy 257 (2023) 164–195, https://doi.org/10.1016/j.solener.2023.04.004.
[3] R. Nasrin, Water/MWCNT nanofluid based cooling system of PVT: experimental and numerical research, Renew. Energy (2018).
[4] A. Nahar, M. Hasanuzzaman, N.A. Rahim, Numerical and experimental investigation on the performance of a photovoltaic thermal collector with parallel plate flow channel under different operating conditions in Malaysia, Solar Energy 144 (2017) 517–528, https://doi.org/10.1016/j.solener.2017.01.041.
[5] T.T. Chow, A review on photovoltaic/thermal hybrid solar technology, Appl. Energy 87 (2010) 365–379, https://doi.org/10.1016/j.apenergy.2009.06.037.
[6] M. Kargaran, H.R. Goshayeshi, H. Pourpasha, I. Chaer, S Zeinali Heris, An extensive review on the latest developments of using oscillating heat pipe on cooling of photovoltaic thermal system, Therm. Sci. Eng. Progr. 36 (2022) 101489, https://doi.org/10.1016/j.tsep.2022.101489.
[7] A. Bianchini, A. Guzzini, M. Pellegrini, C. Saccani, Photovoltaic/thermal (PV/T) solar system: experimental measurements, performance analysis and economic assessment, Renew. Energy 111 (2017) 543–555, https://doi.org/10.1016/j.renene.2017.04.051.
[8] Y. Zhang, C. Shen, C. Zhang, G. Lv, C. Sun, D. Chwieduk, The study of heat control on PVT modules with a new leaf-like heat exchanger, J. Renew. Sustain. Energy 13 (2021) 023703, https://doi.org/10.1063/5.0030541.
[9] Z. Rezvani, H. Mortezapour, M. Ameri, H. Akhavan, Configuration designs and recent applications of photovoltaic-thermal solar collectors for drying agricultural material: a review, BBR 1 (2022), https://doi.org/10.22103/bbr.2022.18904.1002.
[10] A. Fudholi, K. Sopian, M.H. Yazdi, M.H. Ruslan, A. Ibrahim, H.A. Kazem, Performance analysis of photovoltaic thermal (PVT) water collectors, Energy Convers. Manage 78 (2014) 641–651, https://doi.org/10.1016/j.enconman.2013.11.017.
[11] P. Poredoš, U. Tomc, N. Petelin, B. Vidrih, U. Flisar, A. Kitanovski, Numerical and experimental investigation of the energy and exergy performance of solar thermal, photovoltaic and photovoltaic-thermal modules based on roll-bond heat exchangers, Energy Convers. Manage 210 (2020) 112674, https://doi.org/10.1016/j.enconman.2020.112674.
[12] H.A. Kazem, A.H.A. Al-Waeli, M.T. Chaichan, K.H. Al-Waeli, A.B. Al-Aasam, K. Sopian, Evaluation and comparison of different flow configurations PVT systems in Oman: a numerical and experimental investigation, Solar Energy 208 (2020) 58–88, https://doi.org/10.1016/j.solener.2020.07.078.
[13] A. Zabihi Sheshpoli, O. Jahanian, K. Nikzadfar, M Aghajani Delavar, Numerical and experimental investigation on the performance of hybrid PV/thermal systems in the north of Iran, Solar Energy 215 (2021) 108–120, https://doi.org/10.1016/j.solener.2020.12.036.
[14] N. Aste, C. Del Pero, F. Leonforte, Thermal-electrical optimization of the configuration a liquid PVT collector, Energy Procedia 30 (2012) 1–7, https://doi.org/10.1016/j.egypro.2012.11.002.
[15] Adnan Ibrahim, Goh Li Jin, Roonak Daghigh, Mohd Huzmin Mohamed Salleh, Mohd Yusof Othman, Mohd Hafidz Ruslan, Sohif Mat, Kamaruzzaman Sopian, Hybrid Photovoltaic Thermal (PV/T) air and water based solar collectors suitable for building integrated applications, Am. J. Environ. Sci. 5 (5) (2009) 618–624, n.d.
[16] S.K. Verma, K. Sharma, N.K. Gupta, P. Soni, N. Upadhyay, Performance comparison of innovative spiral shaped solar collector design with conventional flat plate solar collector, Energy 194 (2020) 116853, https://doi.org/10.1016/j.energy.2019.116853.
[17] A. Nahar, M. Hasanuzzaman, N.A. Rahim, A three-dimensional comprehensive numerical investigation of different operating parameters on the performance of a photovoltaic thermal system with pancake collector, J. Sol. Energy Eng. 139 (2017) 031009, https://doi.org/10.1115/1.4035818.
[18] A. Shahsavar, Experimental evaluation of energy and exergy performance of a nanofluid-based photovoltaic/thermal system equipped with a sheet-and-sinusoidal serpentine tube collector, J. Clean. Prod. 287 (2021) 125064, https://doi.org/10.1016/j.jclepro.2020.125064.
[19] K. Sopian, G.L. Jin, M.Y. Othman, S.H. Zaidi, M. Hafidz, Advanced absorber design for Photovoltaic Thermal (PV /T) collectors, Recent Res. Energy, Environ. Landsc. Archit. 978-1–6180 (2011) 77–83, n.d.
[20] M. Herrando, A. Ramos, I. Zabalza, C.N. Markides, A comprehensive assessment of alternative absorber-exchanger designs for hybrid PVT-water collectors, Appl. Energy 235 (2019) 1583–1602, https://doi.org/10.1016/j.apenergy.2018.11.024.
[21] M.A. Mohd Rosli, Y.J. Ping, S. Misha, M.Z. Akop, K. Sopian, M. Sohif, et al., Simulation study of computational fluid dynamics on photovoltaic thermal water collector with different designs of absorber tube, J. Adv. Res. Fluid Mech. Therm. Sci. 52 (2018) 12–22.
[22] C. Shen, Y. Zhang, C. Zhang, J. Pu, S. Wei, Y. Dong, A numerical investigation on optimization of PV/T systems with the field synergy theory, Appl. Therm. Eng. 185 (2021) 116381, https://doi.org/10.1016/j.applthermaleng.2020.116381.
[23] H. Ben Cheikh El Hocine, K. Touafek, F Kerrour, Theoretical and experimental studies of a new configuration of photovoltaic–thermal collector, J. Sol. Energy Eng. 139 (2017) 021012, https://doi.org/10.1115/1.4035328.
[24] M.S. Hossain, A.K. Pandey, J. Selvaraj, N.A. Rahim, M.M. Islam, V.V. Tyagi, Two side serpentine flow based photovoltaic-thermal-phase change materials (PVT-PCM) system: energy, exergy and economic analysis, Renew. Energy 136 (2019) 1320–1336, https://doi.org/10.1016/j.renene.2018.10.097.
[25] A. Kazemian, T. Ma, Y. Hongxing, Evaluation of various collector configurations for a photovoltaic thermal system to achieve high performance, low cost, and lightweight, Appl. Energy 357 (2024) 122422, https://doi.org/10.1016/j.apenergy.2023.122422.
[26] J. Ji, G. Pei, T. Chow, K. Liu, H. He, J. Lu, et al., Experimental study of photovoltaic solar assisted heat pump system, Solar Energy 82 (2008) 43–52, https://doi.org/10.1016/j.solener.2007.04.006.
[27] J. Yao, W. Liu, Y. Zhao, Y. Dai, J. Zhu, V. Novakovic, Two-phase flow investigation in channel design of the roll-bond cooling component for solar assisted PVT heat pump application, Energy Convers. Manage 235 (2021) 113988, https://doi.org/10.1016/j.enconman.2021.113988.
[28] A.K. Azad, S. Parvin, Photovoltaic thermal (PV/T) performance analysis for different flow regimes: a comparative numerical study, Int. J. Thermofluids 18 (2023) 100319, https://doi.org/10.1016/j.ijft.2023.100319.
[29] M.M. Rahman, M. Hasanuzzaman, N.A. Rahim, Effects of operational conditions on the energy efficiency of photovoltaic modules operating in Malaysia, J. Clean. Prod. 143 (2017) 912–924, https://doi.org/10.1016/j.jclepro.2016.12.029.
[30] S. Dubey, A.A.O. Tay, Testing of two different types of photovoltaic–thermal (PVT) modules with heat flow pattern under tropical climatic conditions, Energy Sustain. Dev. 17 (2013) 1–12, https://doi.org/10.1016/j.esd.2012.09.001.
[31] R. Nasrin, M. Hasanuzzaman, N.A. Rahim, Effect of high irradiation on photovoltaic power and energy, Int. J. Energy Res. 42 (2018) 1115–1131, https://doi.org/10.1002/er.3907.
[32] E. Skoplaki, J.A. Palyvos, On the temperature dependence of photovoltaic module electrical performance: a review of efficiency/power correlations, Solar Energy 83 (2009) 614–624, https://doi.org/10.1016/j.solener.2008.10.008.
[33] R. Nasrin, M. Hasanuzzaman, N.A. Rahim, Effect of high irradiation and cooling on power, energy and performance of a PVT system, Renew. Energy 116 (2018) 552–569, https://doi.org/10.1016/j.renene.2017.10.004.
[34] M. Alktranee, M.A. Shehab, Z. Németh, P. Bencs, K. Hernadi, T. Koós, Energy and exergy assessment of photovoltaic-thermal system using tungsten trioxide nanofluid: an experimental study, Int. J. Thermofluids 16 (2022) 100228, https://doi.org/10.1016/j.ijft.2022.100228.
[35] S. Bhattarai, J.-H. Oh, S.-H. Euh, G. Krishna Kafle, D Hyun Kim, Simulation and model validation of sheet and tube type photovoltaic thermal solar system and conventional solar collecting system in transient states, Solar Energy Mater. Solar Cells 103 (2012) 184–193, https://doi.org/10.1016/j.solmat.2012.04.017.
[36] H. Fayaz, N.A. Rahim, M. Hasanuzzaman, A. Rivai, R. Nasrin, Numerical and outdoor real time experimental investigation of performance of PCM based PVT system, Solar Energy 179 (2019) 135–150, https://doi.org/10.1016/j.solener.2018.12.057.
[37] H. Bahaidarah, A. Subhan, P. Gandhidasan, S. Rehman, Performance evaluation of a PV (photovoltaic) module by back surface water cooling for hot climatic conditions, Energy 59 (2013) 445–453, https://doi.org/10.1016/j.energy.2013.07.050.
[38] H.G. Teo, P.S. Lee, M.N.A. Hawlader, An active cooling system for photovoltaic modules, Appl. Energy 90 (2012) 309–315, https://doi.org/10.1016/j.apenergy.2011.01.017.
[39] M. Chandrasekar, S. Suresh, T. Senthilkumar, M Ganesh Karthikeyan, Passive cooling of standalone flat PV module with cotton wick structures, Energy Convers. Manage 71 (2013) 43–50, https://doi.org/10.1016/j.enconman.2013.03.012.
[40] H. Fayaz, N.A. Rahim, M. Hasanuzzaman, R. Nasrin, A. Rivai, Numerical and experimental investigation of the effect of operating conditions on performance of PVT and PVT-PCM, Renew. Energy 143 (2019) 827–841, https://doi.org/10.1016/j.renene.2019.05.041.
[41] L.W. Florschuetz, Extension of the Hottel-Whillier model to the analysis of combined photovoltaic/thermal flat plate collectors, Solar Energy 22 (1979) 361–366, https://doi.org/10.1016/0038-092X(79)90190-7.
[42] B. Podder, A. Biswas, S. Saha, Multi-objective optimization of a small sized solar PV-T water collector using controlled elitist NSGA-II coupled with TOPSIS, Solar Energy 230 (2021) 688–702, https://doi.org/10.1016/j.solener.2021.10.078.
[43] Y. Yu, H. Yang, J. Peng, E. Long, Performance comparisons of two flat-plate photovoltaic thermal collectors with different channel configurations, Energy 175 (2019) 300–308, https://doi.org/10.1016/j.energy.2019.03.054.

Yassine El Alami was born in 1997 in Oum Rabia, Morocco. He has had a remarkable academic career, beginning with his bachelor's degree in Experimental Sciences in 2016. In 2020, he completed his Bachelor of Science in Physical Matter Science, specializing in Energy Physics, at the Faculty of Sciences of Moulay Ismail University, located in Meknes, Morocco. In 2022, Yassine continued his studies by obtaining a Master's degree from the Faculty of Science at the Chouaïb Doukkali University, in El-Jadida, Morocco. In 2022, Yassine El Alami took a new turn in his academic career by joining the Chouaïb Doukkali University, in El-Jadida, Morocco, as a Ph.D. student in the Electronics, Instrumentation, and Energetics (LEIE) program. His research focuses on the experimental characterization and simulation of photovoltaic-thermal (PVT) hybrid generators.

Ali Lamkaddem was born in Al-Hoceima, Morocco in 1990. He obtained his PhD degree in Physics and Engineering Specialty: Electronics, Power Electronics and Renewable Energies at Mohamed First University, Oujda - Morocco in 2021. He published more than of 30 publications and international communications in the field of photovoltaic renewable energies. In addition, his research interests include the improvement of photovoltaic systems (DC/DC and DC/AC converters) dedicated to renewable energies.

Rachid Bendaoud was born in El Jadida City (Morocco) in 1984. obtained his Ph.D. degree in Electronics and renewable energy from Chouaib Doukkali University, Morocco in 2019. His Ph.D. work aimed to contribution to the experimental characterization of the PV generator: modeling and new method for extracting physical parameters. Then, in 2022, he integrated the Higher School of Education and training of Berrechid, Hassan 1st University as Professor researcher. His research and interests focus on the power electronics, photovoltaic energy, thermal, electronic system, electrical engineering, optimization, cooling systems for PV systems.

Name: Sofian Surname: Talbi Birthday: 07.04.1990 Birth Place: Bouyafer, Nador, Morocco Bachelor: Science of Physical Matter, Mechanical Option, Department of Physics, Faculty of Sciences, University of Mohamed I, Oujda, Morocco, 2012 Master: Renewable Energies, Department of Physics, Faculty of Sciences, University of Mohamed I, Oujda, Morocco, 2014 International Journal on "Technical and Physical Problems of Engineering" (IJTPE), Iss. 56, Vol. 15, No. 3, Sep. 2023 233 Doctorate: Energetic Physics and Renewable Energies, Department of Physics, Faculty of Sciences, University of Mohamed I, Oujda, Morocco, 2020 The Last Scientific Position: Assist. Prof, Department of physics, Higher Education at Multidisciplinary Faculty, University of Mohammed I, Nador, Morocco, 2021 Research Interests: Energy Physics and Renewable Energies Scientific Publications: 14 Papers, 1 Thesis.

Mohamed Louzazni received the B.Sc.degree in electronics from the Faculty of Science, Ibn Tofail University, the M.Sc. degree in electronics and telecommunication from the Faculty of Science, Abdelmalek Essaâdi University, and the Ph.D. degree in electrical and renewable energy engineering from the National School of Applied Science, Tangier. He was a visiting Ph.D. student with the Faculty of Electrical Engineering, University Polytechnic of Bucharest, in 2015. In 2017, he started his research at the Solar Tech Laboratory, Energy Department, University Polytechnic of Milan, Italy. In 2018, he was a Ph.D. visitor at the Higher Polytechnic School of Algeciras, University of Cadiz, Spain, for _ve months. He is currently a Researcher with Chouaib Doukkali University. His research interests include mathematical modeling, optimization, meta-heuristic algorithm, computational intelligence, photovoltaic and power energy, forecasting, fuel cell, GPR, radio frequency, electromagnetic, and electronic.

Elhadi Baghaz was born in Al Hoceima City (Morocco) in 1985. obtained his Ph.D. degree in Electronics and renewable energy from Mohammed First University, Morocco in 2015. His Ph.D. work aimed to discretized architectures for managing the energy supplied by photovoltaic systems. Then, in 2018, he integrated the Laboratory of Electronics, Instrumentation and Energetics at the Faculty of Science of El jadida, University Chouaïb Doukkali as Professor researcher. His research and interests focus on the power electronics, photovoltaic energy, thermal, electronic system, electrical engineering, optimization, cooling systems for PV systems.